To appear in:
The New Optics
Cambridge University Press

Laser Cooling and Manipulation of Neutral Particles

Charles S. Adams and Erling Riis

I. INTRODUCTION

Some of the most significant advances in technology and our basic understanding of physics are based on controlling the motion of *charged* particles using external fields. The vacuum tube and transistor exploit our ability to control the motion of the electron, while particle accelerators provide the means to study the basic constituents of matter. In contrast our ability to control the motion of *neutral* particles is vastly more limited. For example, if we wish to hold an object there is no significant force until our fingers are within a few atomic diameters of its surface. Recently, due to the development of lasers, our potential to control neutral particles at a distance has been greatly extended. Lasers can trap both macroscopic particles, a technique known as optical *tweezers*, and cool atoms to within a millionth of a degree of absolute zero. At such low temperatures they become easy to manipulate with external fields. These techniques are beginning to have a profound impact in many areas of physics, chemistry and biology, earning the Nobel prize for three of their pioneers (Cohen-Tannoudji, Phillips, and Chu) in 1997.

This Chapter begins with a brief history (Sec. II), then discusses the basic physical principles underlying light forces (Sec. III), laser cooling (Sec. IV) and trapping of neutral particles (Sec. V). Finally some applications of these techniques in atomic physics (Sec. VI) and in the study of micron sized particles (Sec. VII) are discussed.

II. HISTORICAL SKETCH

A. The mechanical effects of light

The idea that light may affect the motion of matter originated with Kepler, who incorrectly conjectured that comets tails were repelled by a solar light pressure. Subsequent attempts to measure this pressure proved inconclusive. For example, in 1875 (soon after Maxwell had provided theoretical support to the concept) Crookes demonstrated his now famous light radiometer to members of the Royal Society: His instrument, still sold as a curiosity, consisted of an evacuated bulb containing a freely suspended vane. Alternate faces of the vane were coated black and silver such that the reflection and absorption of light should cause it to spin. When illuminated by a bright light the vane did indeed spin but in the wrong direction, due to the thermal 'convection' of residual gas molecules. In 1901 Lebedev in Moscow, and Nichols and Hull at Dartmouth College in New Hampshire succeeded in reducing the background pressure and outgasing from the vanes to a level required to observe the correct rotation predicted by Maxwell.

An important step towards our present understanding of radiation pressure was made in 1917 by Einstein, who showed that a quantum of light, or *photon*, with energy $h\nu$, carries a momentum, $h\nu/c = h/\lambda$, where h is Planck's constant, c, ν, and λ are the speed, frequency, and wavelength of the light respectively. The particle-like nature of radiation was reinforced in the early 1920's by the experimental demonstration of the Compton effect where electrons are scattered by high-frequency photons (X-rays). Although the recoil of

an atom produced by scattering a single optical photon is substantially smaller, the radiation pressure on atoms can be much larger due to the resonant nature of the process. The first experimental demonstration of a light pressure on atoms was reported in 1933 by Frisch in Hamburg. He illuminated a thermal Na beam with resonant light from a Na lamp and observed a slight deflection away from the lamp, consistent with an estimate that one third of the atoms were excited. The low excitation rate was due to the low spectral brightness of the light source, a problem that would remain a fundamental limitation until the invention of the laser.

B. Early laser experiments

The advent of lasers would completely revolutionise the potential for manipulating particles using light, however theoretical proposals preceded the first experiments. In 1962, Askar'yan showed that *intensity gradients* could exert substantial forces on atoms due to the induced dipole moment. In 1968, Letokhov suggested that this dipole force could be used to trap atoms at the nodes (or anti-nodes) of a standing wave light field detuned far from the atomic resonance. In the early 1970s, Ashkin at Bell Laboratories trapped small glass spheres between opposing focused laser beams, and levitated a bead using a single beam. By accident Ashkin discovered that the trap could be used to hold live cells (see Sec. VII). Ashkin realised that light forces can be divided into two classes (Sec. III A), the *spontaneous force* arising from the absorption and spontaneous emission of photons, and the *dipole force* discussed by Askar'yan. Following the development of tunable dye lasers in 1972, laser based versions of Frisch's experiment were performed producing a significantly larger deflection. However, optical trapping of neutral atoms remained elusive. Atom trapping required a means to slow the atoms down to a kinetic energy less than the depth of the light trap.

In 1975 Hänsch and Schawlow, and independently Wineland and Dehmelt, realised that laser light could potentially be used to cool atoms and ions, respectively. In both cases the cooling mechanism was based on the Doppler effect and so became known as *Doppler cooling* (see Sec. IV A). As room temperature atoms move at the speed of supersonic aeroplanes, the first experiments concentrated on slowing an atomic beam using a counter-propagating laser beam. Techniques were developed to maintain a high scattering rate of photons. This included preventing the atoms from decaying into states which were uncoupled to the cooling laser, and compensating for the change in the Doppler shift as the atoms were slowed. In 1982 Phillips and colleagues at NBS (now NIST) were able to slow a thermal sodium atomic beam from 1100 m/s to 40 m/s. In 1985 Chu and co-workers at Bell Labs went one step farther. They managed to cool slow sodium atoms using three orthogonal pairs of counter-propagating laser beams. This configuration, dubbed *optical molasses*, resulted in a final temperature of approximately 240 μK.

The extreme low temperatures resulting from laser cooling suddenly made atom trapping easy. Atoms from a laser cooled atomic beam were trapped by a magnetic field (see Sec. V A) at NIST in 1985. A year later at Bell Labs, optical molasses was used to load a trap made from a single focused laser beam (see Sec. V B). In 1987 a much deeper trap, known as the magneto-optical trap (or MOT) (see Box 4) was demonstrated for atoms. The MOT has now become a common starting point in most laser cooling experiments.

The field of laser cooling continued to develop rapidly during the late 1980's. In 1988 the NIST group discovered that the temperature of atoms in optical molasses were significantly *lower* than the so-called Doppler limit predicted by two-level atom theory (see Fig. 1). Soon after the groups of Cohen-Tannoudji in Paris and Chu in Stanford realised that the multi-level character of real atoms and the spatial variation of the polarisation of the light field played an important role in the cooling process. Atoms cooled by this new mechanism, (known as sub-Doppler or *polarisation gradient cooling*, see Sec. IV B) end up with a mean velocity υ_{rms} as low as 3-5 υ_{rec} , where υ_{rec} is the velocity an atom gains on the emission of a single photon. The typical temperature range for a number of cooling mechanisms is illustrated in Fig. 1.

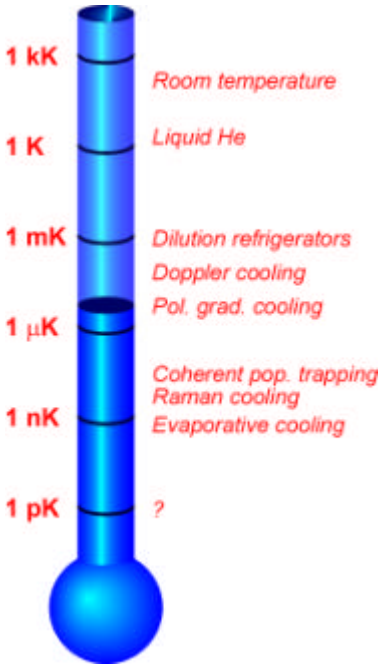

Fig. 1. *The temperature scale relevant to laser cooling. The main cooling mechanisms and their characteristic temperatures are indicated.*

C. Recent advances in laser cooling and trapping.

In 1988 Aspect and co-workers at the ENS in Paris demonstrated that it was possible to cool atoms below the *recoil limit* $\upsilon_{rms} = \upsilon_{rec}$. Their sub-recoil cooling scheme relies on the stochastic nature of spontaneous emission to enable the atoms to randomly walk into a select region of velocity space (with dimension less than υ_{rec}) where subsequently they are left alone (see Sec. IV C). In more recent experiments temperatures below 100 nK have been produced (see Fig. 1). A different sub-recoil cooling scheme based on stimulated Raman transitions was developed by Kasevich and Chu at Stanford in 1992 (see Sec. IV C).

The production of cold atoms by laser cooling soon led some to interesting developments. First, atoms make excellent sensors as exemplified by the atomic clock (see Sec. VI A). The sensitivity of any precision measurement is determined by the signal-to-noise ratio and the interaction time. One of the major contributions of laser cooling has been to significantly increase the interaction time. During a measurement, the atoms must remain in a perturbation free environment, i.e., free fall. This means that on earth the longest interaction times are accomplished using a fountain geometry. The first *atomic fountain* was demonstrated at Stanford in 1989 and the technique has become the standard for the next generation of atomic clocks. Atomic fountains are also ideally suited for other precision measurements such as the Doppler shift of a falling atom (atomic gravitometer, see Sec. VI A).

A second important goal of laser cooling is to increase the 'brightness' or phase-space density of the sample. The phase-space density defines the number of atoms with a given position and momentum. A high phase-space density is an advantage for most experiments in atomic physics and determines whether the sample behaves as *a classical or a quantum fluid* (see Sec. VI B). Laser cooling can dramatically increase the phase space density, but so far not quite by enough to enter the quantum regime. However, in 1995 three groups transferred their laser cooled atoms to a purely magnetic trap and continued to cool by forced evaporation (a technique originally developed for magnetically trapped hydrogen in the 1980's) (see Fig. 1). This led to the first observation of Bose-Einstein condensation in a dilute atomic vapour. A pure Bose condensate represents the 'ultimate' cooling. If all the atoms are in the lowest energy level, then temperature, in the usual sense of a distribution amongst energy levels, loses its meaning.

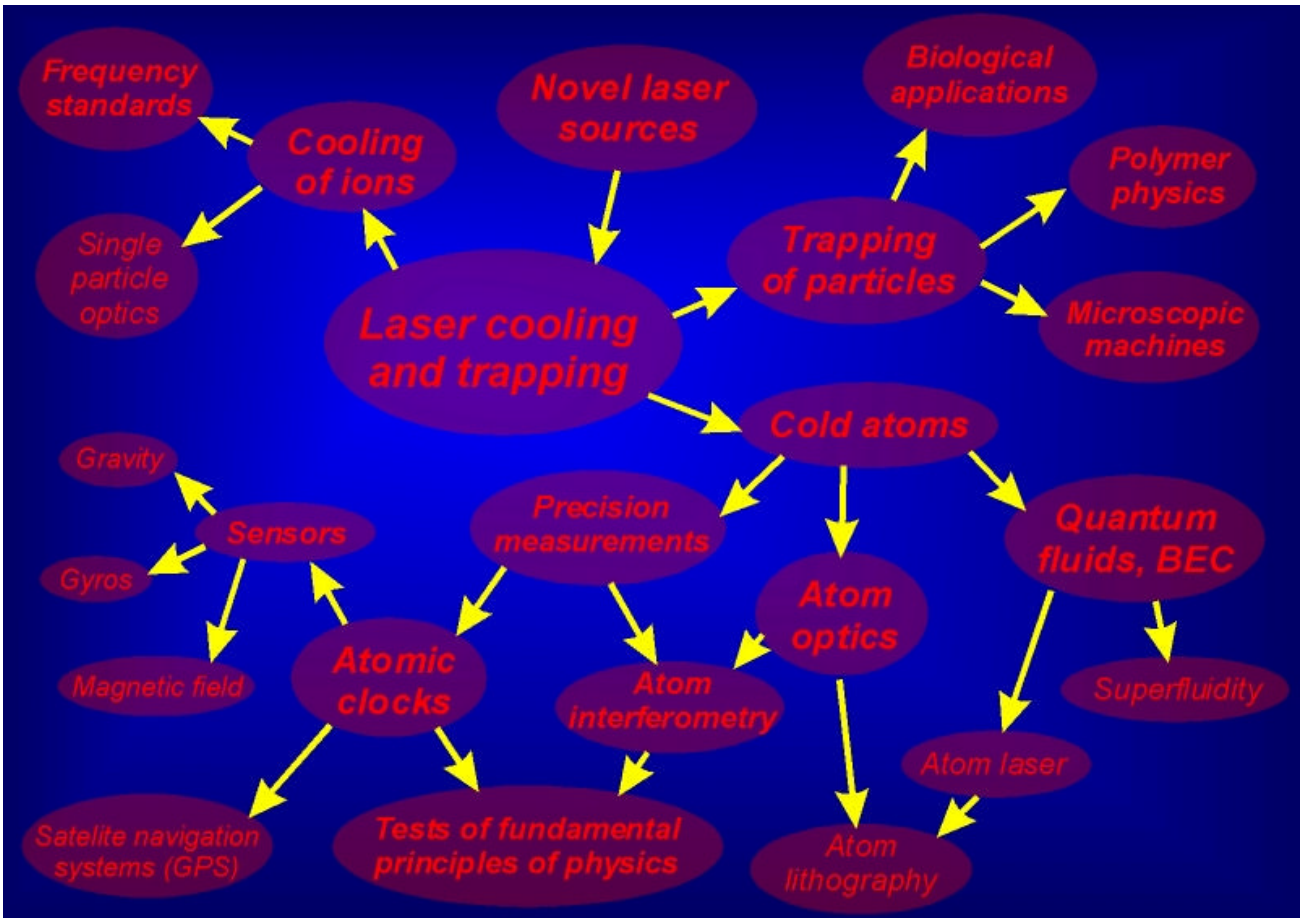

Fig. 2. *Laser cooling is a central part of modern optics. Several of these research fields are described in other Chapters of this book.*

Laser cooling and trapping has developed into a central part of modern optical physics. Fig. 2 illustrates the link to the most important applications as well as connections with related areas of physics, some of which are reviewed in other Chapters of this book.

III. LIGHT FORCES

There are a number of ways of understanding the force exerted by light on matter. Although they all describe the same fundamental physics, it is more appropriate to consider a particle as a refractive polarisable 'optical element' (discussed in Sec. III A), and an atom as a quantum oscillator (Sec. III B).

A Light forces on particles.

The light force on a particle can be seen as a direct consequence of the refraction and absorption of light. Fig. 3a shows a transparent dielectric sphere placed slightly off-axis in a laser beam with a Gaussian intensity profile. If the sphere has a refractive index larger than the surrounding medium, the light is refracted towards the centre of the sphere (to the left in Fig. 3a), therefore the light gains momentum in this direction. Newton's third law implies that the particle experiences a force in the opposite direction. The force can be divided up in two components: a scattering force, F_{scat}, in the direction of the beam, which would be present even in the case of a plane laser wave; and a gradient or dipole force, F_{dip}, directed towards the centre of the beam. The forces due to surface reflections are negligible. If the refractive index of the particle is lower than that of the surrounding medium, the light is refracted in the opposite direction, and the light force tends to push the particle away from the high-intensity region of the beam. If the particle is slightly

absorbing, corresponding to the refractive index having an imaginary component, part of the incoming light momentum is transferred directly to the particle and provides an increased scattering force (radiation pressure).

The same reasoning leads to a slightly different result in the case of a transparent particle near a tight focus as shown in Fig. 3b. Refraction in the sphere tends to collimate a strongly diverging beam resulting in an increase in the light momentum along the propagation direction. By applying Newton's third law we find a dipole force that tends to pull the particle towards the focus. If the particle is absorbing, the scattering force will push the equilibrium position slightly in the propagation direction.

For particles in the micron range and achievable laser intensities the dipole force is substantial: it can be thousands of times larger than gravity. Consequently, it is possible to pick up a dielectric sphere and levitate it with a downward propagating beam as demonstrated in the photograph in Fig. 3c.

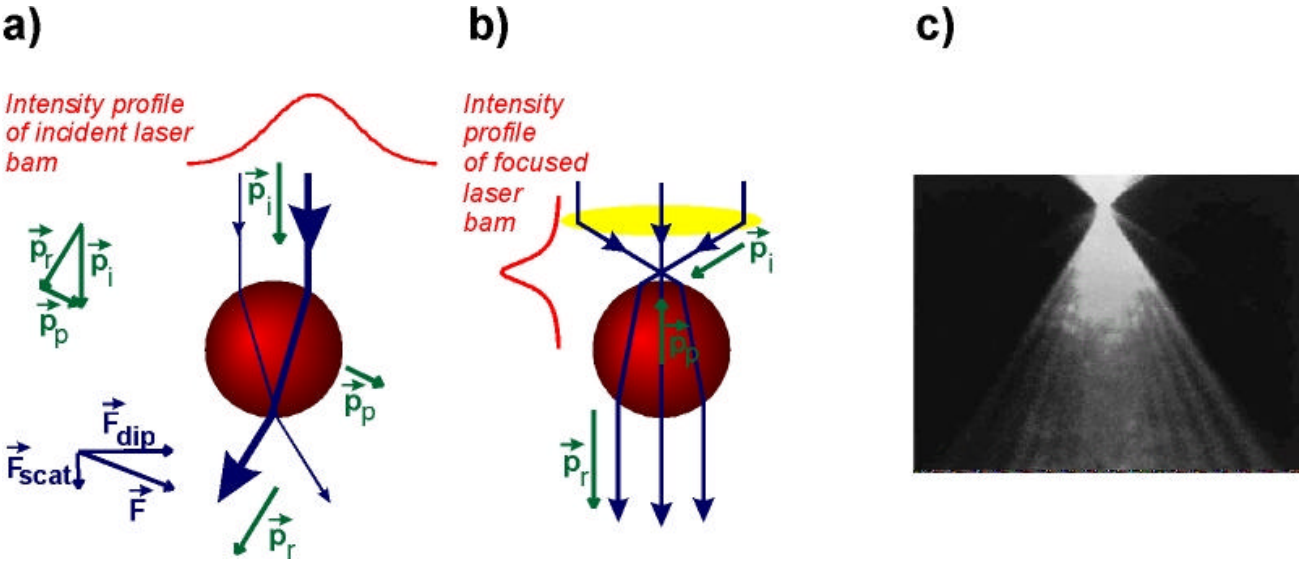

Fig. 3. *Optical forces on a dielectric sphere: a) The sphere is placed off-axis in a collimated laser beam with Gaussian transverse profile. The light is refracted such that the incoming momentum, $\vec{p}_i$, is changed to $\vec{p}_r$. The difference, $\vec{p}_p$, is picked up by the particle and felt as a force, $\vec{F}$, pushing the sphere towards the beam axis ($\vec{F}_{dip}$) and along the propagation direction ($\vec{F}_{scat}$); b) The sphere is placed near a focused beam. Refraction now results in a force towards the focus; c) Photograph of a 10 micron glass sphere trapped in water with green light from an argon laser using the set-up shown in b). The picture is a fluorescence image taken using a green blocking, red transmitting filter. (Photograph courtesy of S. Chu).*

B Light forces on atoms: Photon picture

The basic mechanism underlying the light force on atoms is the conservation of energy and momentum during the absorption and emission of light. As for macroscopic particles, light forces can be divided into two types: the scattering force which is now seen as a result of cycles of absorption and *spontaneous emission*; and the dipole force, which arises due to cycles of absorption and *stimulated emission*. We will consider the scattering force first. If an atom of mass m absorbs a photon, the energy $h\nu$ is almost entirely converted into internal energy, i.e., the atom ends up in an excited state. The momentum, however, causes the atom to recoil in the direction of the incoming light and change its velocity $\boldsymbol{u}$ by an amount $\hbar\boldsymbol{k}/m$. The atom soon returns to the ground state by spontaneously emitting a photon. The conservation of momentum in this process causes the atom to recoil again, this time in the opposite direction to the emitted photon.

However, as spontaneous emission is a random process with a symmetric distribution, it does not contribute to the net change in momentum when averaged over many absorption and spontaneous emission cycles or a large sample of atoms. Fig. 4a illustrates how an atom, on average, changes its velocity by an amount $\hbar \boldsymbol{k}/m$ each time it runs through this cycle. The time averaged scattering force is given by Newton's second law,

$$\boldsymbol{F} = \frac{\Delta \boldsymbol{p}}{\Delta t} = \frac{\hbar \boldsymbol{k}}{\tau / f_e}$$

where τ is the natural lifetime of the excited state, and f_e is the fraction of atoms in the excited state. For the Na resonance transition, τ = 16 ns, and the maximum acceleration (corresponding to f_e = 0.5, see Box 1) is 10^6 m/s^2 or 10^5 g! So even though a single photon recoil is relatively small, the radiation pressure can be enormous because on resonance the atom scatters 30 million photons per second.

BOX 1

Absorption and emission of near-resonant light

In the simplest laser cooling scenario, the laser is tuned close to resonance with a transition from the ground state to a single excited state which decays by spontaneously emission back to the ground state. If the laser is exactly on resonance and there is no spontaneous emission, the atom undergoes cycles of absorption and stimulated emission, and the population oscillates between the ground and excited state at the frequency, ω_R, known as the *Rabi frequency* (as illustrated by the blue curve in Fig. B1a - see also Box 3). Spontaneous emission interrupts these Rabi oscillations by resetting the excited state component of the atomic state to zero (the red curve in Fig. B1a, simulated using a Monte-Carlo wavefunction). If one averages over many atoms, then the net effect of spontaneous emission is to damp the Rabi oscillations towards a steady-state excited state population (the green curve in Fig. B1a). The steady-state fraction, f_e, increases with intensity, approaching 1/2 for high intensity (Fig. B1b). This saturation effect sets the maximum value of the spontaneous light force.

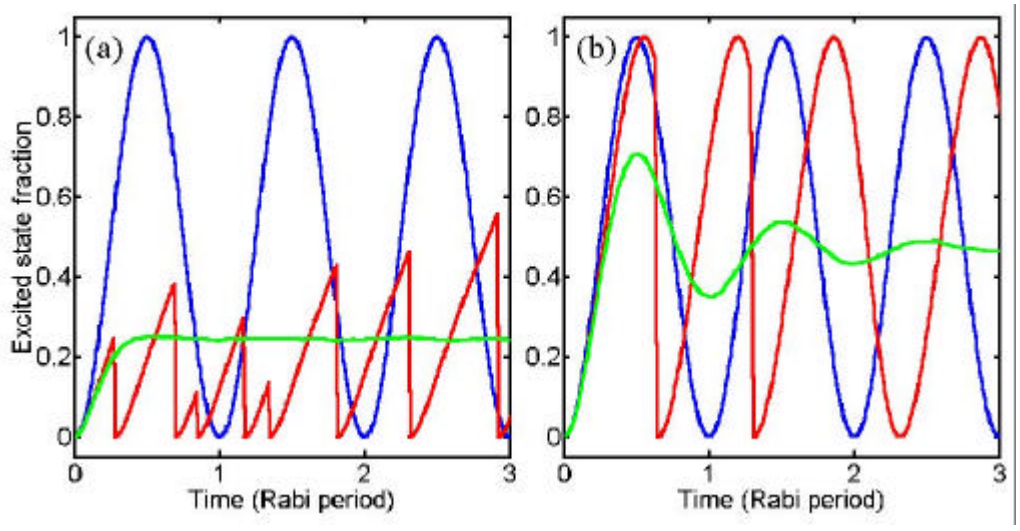

Fig. B1. *Simulations of a two-level atom in a resonant laser field. With no spontaneous emission (blue), the atomic population oscillates between the ground and excited state at the Rabi frequency. Spontaneous emission interrupts the Rabi cycle and resets the excited state probability to zero (red). By averaging over many atoms (10000 in this example) one obtains the steady-state fraction, f_e (green). (a) At the saturation intensity corresponding to $\omega_R = \Gamma/\sqrt{2}$, f_e = 1/4. (b) At high intensity, ω_R = 3.3 Γ, f_e approaches 1/2.*

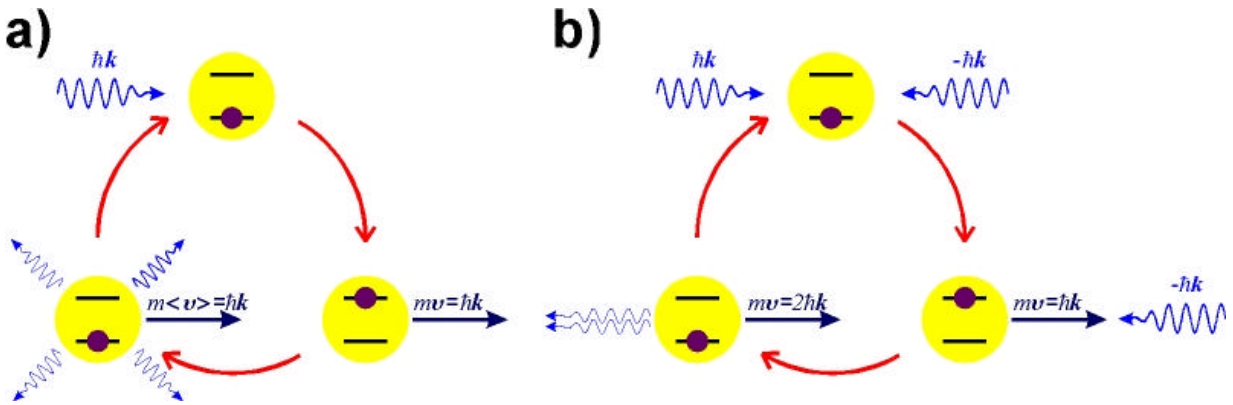

Fig. 4. *Photon picture of the light forces on atoms: (a) The scattering force: A two-level atom, initially in the ground state (top), absorbs a photon with momentum* $\hbar\mathbf{k}$. *The excited atom increases its velocity by* $\hbar\mathbf{k}/m$, *in the direction of the incoming beam. The internal atomic energy is released by spontaneous emission of a photon, in a direction described by a symmetric probability distribution, so the average velocity change is zero. The atom returns to the ground state, ready to start the cycle over again; (b) The dipole force due to stimulated emission. The atom absorbs a photon and gains a momentum* $\hbar\mathbf{k}$ *It is then stimulated back to the ground state by a photon from the opposite direction gaining a further* $\hbar\mathbf{k}$ *of momentum.*

The dipole force arises due to the interaction between the induced atomic dipole moment and the electric field of the laser (see Boxes 2 and 3), however, a simple intuitive picture can be gained by considering the momentum exchange during cycles of absorption and stimulated emission as depicted in Fig. 4b. If the atom initially absorbs a photon from the left it can be stimulated to emit to the left inducing a momentum change of $2\hbar\mathbf{k}$. This coherent redistribution of photons is produced by the interference between the incident and emitted light occurring in a field gradient, hence the alternative name, the *gradient* force.

IV. LASER COOLING OF NEUTRAL ATOMS

A. Doppler cooling

The ability to use laser radiation to cool atoms was first proposed by Hänsch and Schawlow in 1975. The idea was to illuminate an atom from all directions with light tuned slightly below an atomic absorption line. A moving atom sees oncoming light Doppler shifted closer to resonance, whereas co-propagating light is shifted away from resonance. Consequently, the atom predominantly scatters from the forward direction and is slowed down. Fig. 5 illustrates the effect in a one-dimensional (1-D) situation. As the Doppler effect plays a central role in the process it is normally referred to as Doppler cooling. The cooling force for 1-D Doppler cooling can be determined from the expression in the previous section by considering the force from each beam independently,

$$F = \frac{\hbar k}{\tau / f_-} - \frac{\hbar k}{\tau / f_+}$$

where $f_\pm/\tau$ is the scattering rate from the two beams,

$$f_\pm = \frac{I/2I_{sat}}{4\tau^2(\Delta \mp k\upsilon)^2 + (1 + 2I/I_{sat})}$$

where I_{sat} is the intensity corresponding to a resonant atom spending 1/4 of its time in the excited state (see Box 1).

BOX 2

Classical field picture.

An alternative description of the light force on atoms, in particular a more accurate picture of the dipole or gradient force, is provided by considering the interaction between the electric field $\boldsymbol{E} = \boldsymbol{E_0}\cos(\omega_L t + \varphi)$ and induced atomic dipole moment $\boldsymbol{d}$. The interaction energy is given by

$$U = -\boldsymbol{d}\cdot\boldsymbol{E}$$

If we ignore spontaneous emission for the moment, the atomic dipole behaves similarly to any classical oscillator, e.g. a mass on a spring, with a oscillation frequency determined by the energy level spacing $\omega_0 = (E_e - E_g)/\hbar$ where E_g and E_e are the ground and excites states energies respectively. The laser acts as an external driving field. If the driving frequency ω_L is less than ω_0 (referred to as red detuning) the atomic dipole oscillates in phase. In this case, the interaction energy U is negative and the atom is attracted towards maximum intensity. In contrast, if the driving frequency ω_L is greater than ω_0 (blue detuning) the interaction energy is positive and the atom is repelled from maximum intensity. Exactly on resonance, the dipole moment and the electric field are orthogonal so the net force should be zero, however, in this case spontaneous emission is also important.

To include the effect of spontaneous emission we write that

$$d = E_0\left(\alpha' cos(\omega_L t) - \alpha'' sin(\omega_L t)\right)$$

which states that the atomic dipole moment d oscillates with an amplitude proportional to that of the driving field, E_0, and at the same frequency but not necessary in phase, α' and α'' play the roles of the real and imaginary parts of the atomic 'refractive' index (in analogy to Sec III A).

The time-averaged force is given by the gradient of the potential and can be written as:

$$F = \langle -\nabla U\rangle = -\frac{1}{2}\alpha'\,\nabla E_0^2 - \frac{1}{2}\alpha''\,E_0^2\,\nabla\varphi$$

where $\alpha' E_0$ and $\alpha'' E_0$ are the steady state in-phase and quadrature components of the induced atomic dipole moment. The force has two components: The first term, proportional to the gradient of the intensity,

$$F_{dip} = -\frac{1}{2}\alpha'\nabla E_0^2$$

is the gradient force or dipole force, and can be positive or negative depending on the sign of the detuning as discussed above; and the second term, proportional to the gradient of the phase,

$$F_{scat} = -\frac{1}{2}\alpha'' E_0^2\nabla\varphi$$

is the radiation pressure force or scattering force.

BOX 3

Dressed atom picture: the light shift.

In Box 2 we considered the light forces from the point of view of the classical electro-magnetic field. It is also very instructive to consider the dipole force from an atomic or quantum mechanical point of view. The laser is tuned by an amount Δ below resonance with an atomic transition between a ground state energy level labelled $|g\rangle$ and an excited state level labelled $|e\rangle$ (see Fig. B3a). These two states are coupled by the interaction of the atomic dipole moment ***d*** with the electric field ***E*** of the laser:

$$V_{A-L} = -\boldsymbol{d}\cdot\boldsymbol{E}$$

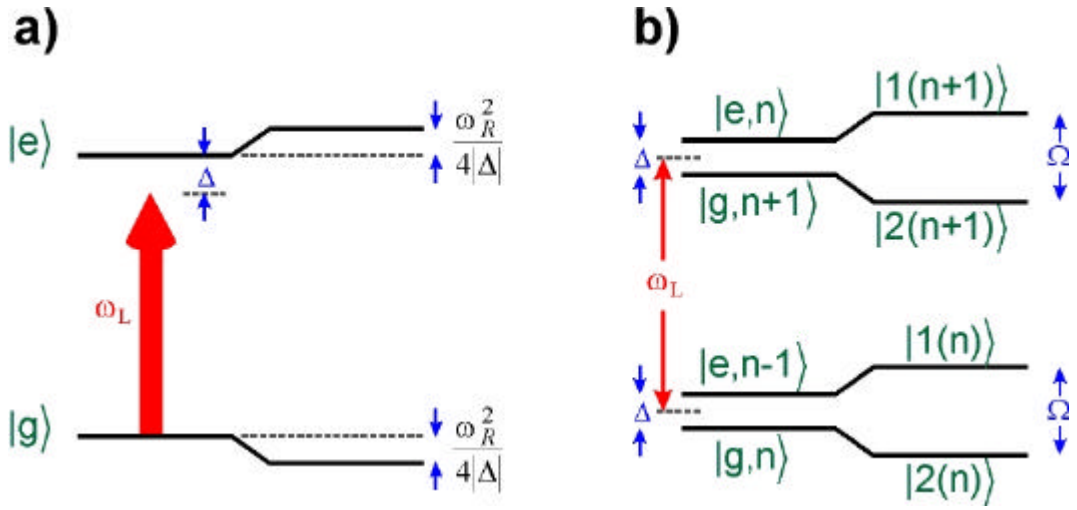

Fig. B3. *The light shift: (a) Two atomic levels $|g\rangle$ and $|e\rangle$ are coupled to a laser field with frequency ω_L. The coupling strength is characterised by the Rabi frequency, ω_R. If the laser is tuned below resonance, the two levels repel. This is known as the light shift or ac-Stark effect. For $|\Delta| >> \omega_R$, the light shift is given by $\omega_R^2/4|\Delta|$; (b) In the dressed atom picture, the energy of the atom and the laser field are added together: the energy of a ground state atom, $|g\rangle$, and n photons in the field is close to that of an excited state atom $|e\rangle$ and n-1 photons. For increasing photon number, the dressed energy levels form a ladder of manifolds, each containing two states. The atom-field interaction splits the levels within a manifold by an amount $\hbar\Omega = \hbar\sqrt{\Delta^2 + \omega_R^2}$. The eigenstates of the coupled system ($|1(n)\rangle, |2(n)\rangle$, etc.) are linear combinations of the uncoupled states ($|g,n\rangle, |e,n-1\rangle$, etc.).*

The correct quantum mechanical treatment of the problem is to consider the atom and field as one system - the dressed atom picture. Ignoring the interaction for the moment, the states of the combined system are characterised by the atomic state ($|g\rangle$ or $|e\rangle$) and the number of photons, n, in the laser field. The energy levels therefore form a ladder of manifolds separated by the photon energy $\hbar\omega$ and each containing two states of the form $|g,n\rangle$ and $|e,n-1\rangle$. The left-hand side of Fig. B3b shows two steps of the ladder for a laser field tuned below resonance. If the light-atom interaction is turned-on, the eigenstates of the system (labelled $|1(n)\rangle$ and $|2(n)\rangle$) become mixtures of the basis states: ***……continued……***

BOX 3 (continued)

$$|1(n)\rangle = \cos\theta\,|e,n-1\rangle - \sin\theta\,|g,n\rangle$$
$$|2(n)\rangle = \sin\theta\,|e,n-1\rangle + \cos\theta\,|g,n\rangle$$

where $tan\,2\theta = -\omega_R/\Delta$, $\omega_R = 2\langle e,n-1|V_{A-L}|\,g,n\rangle/\hbar$ is the Rabi frequency and characterises the strength of the interaction (see Box 1). The atom is no longer either in the ground state or the excited state; it is in a superposition of both. The interaction causes the levels to repel so that the dressed states are separated by an amount:

$$\hbar\Omega = \hbar\sqrt{\Delta^2 + \omega_R^2}$$

For $\omega_R << \Delta$, state $|2(n)\rangle$, which in the limit of low intensity corresponds to the ground state for a detuning below resonance, is shifted down in energy by an amount proportional to $I/|\Delta|$, where I is the laser intensity. This is known as the light shift or ac-Stark shift. The light field therefore forms a potential well with a depth proportional to intensity. For positive, i.e., blue detuning, state $|1(n)\rangle$ corresponds to the ground state and the atoms experience a potential hill (see Box 2). The dipole force is equal to the gradient of the light shift.

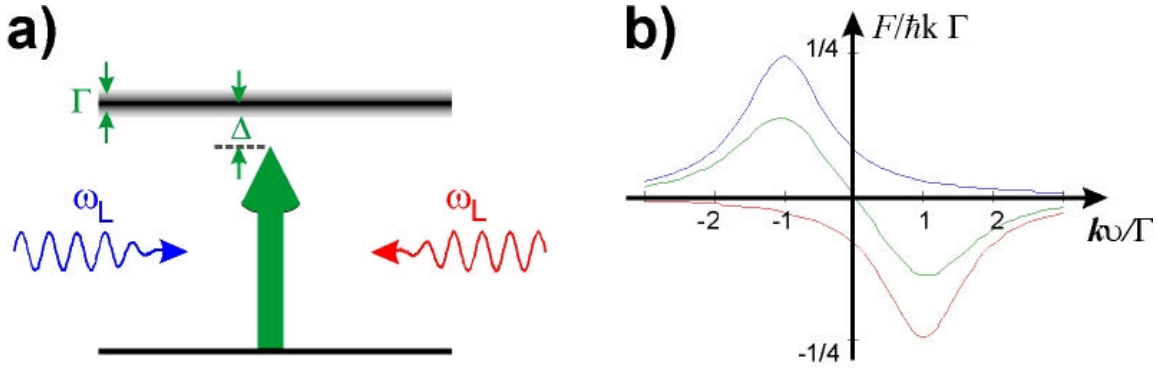

Fig. 5. *One-dimensional Doppler cooling: (a) The frequency of the standing laser field ω_L is detuned by an amount Δ below the resonance with a transition to an excited state, which has a linewidth, Γ, equal to the inverse of the natural lifetime of the excited state; (b) Each of the counter-propagating beams exerts a force with a Lorentzian velocity dependence (red and blue curves). For an intensity equal to the saturation intensity the maximum force corresponds to one photon momentum transferred every four natural lifetimes. The green curve shows the combined force from the two beams, displaying the viscous damping around $\upsilon = 0$.*

As shown in Fig. 5b near $\upsilon = 0$ the force varies linearly with velocity:

$$F = -\alpha\upsilon$$

where α is referred to as the friction coefficient. This is characteristic of a viscous medium where the velocity is damped exponentially towards $\upsilon = 0$. However, similar to a particle in a liquid, the motion never completely stops due to Brownian motion, the stochastic nature of the absorption and spontaneous emission processes put a lower limit on the width of the atomic velocity distribution. In the limit of low intensity, the minimum temperature is given by,

$$T_{\min} = \hbar\Gamma / 2k_B$$

where k_B is Boltzmann's constant and $\Gamma=1/\tau$. The minimum temperature occurs at a red detuing equal to half the transition linewidth, $\Delta = -\Gamma/2$. For the resonance transition in Na, $T_{\min} \approx 240\ \mu K$.

The extension of Doppler cooling to three dimensions is simple. By using six beams, forming three orthogonal standing waves, an atom will everywhere experience a viscous damping force $\vec{F} = -\alpha\vec{v}$ opposing its motion. The first experimental demonstration of 3-D Doppler cooling was reported by Chu in 1985. The experiment was able to confine around 10^5 atoms by radiation pressure, enough that the cloud was clearly visible by eye, see Fig. 6. Due to its viscous nature, it was christened optical molasses. By turning the cooling light off for a variable length of time (a few ms), and detecting the loss of atoms from a given volume due to ballistic expansion, the temperature was estimated to be $T = 240^{+200}_{-60}\ \mu K$, in agreement with the theoretical prediction.

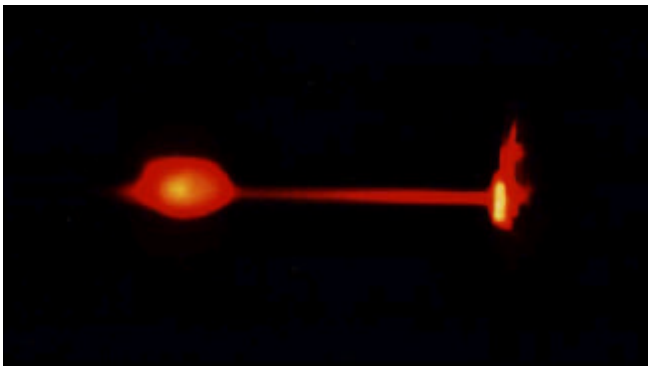

Fig. 6. *Photograph showing atoms confined in optical molasses (right). The atomic beam, originating from the nozzle to the left, is slowed with a counter-propagating laser beam. The atoms are cooled further in optical molasses. The distance from the nozzle to the optical molasses is 5 cm. (Photograph courtesy of S. Chu).*

Although the atoms in 3-D optical molasses are subject to strong viscous damping they are still free to diffuse around (as in Brownian motion). Eventually they wander to the limit of the interaction region where they are lost. However, a simple and extremely important extension to 3-D optical molasses (adding a magnetic field), turns it into a genuine trap, known the magneto-optical trap. Its ease of use and versatility has made this the most widely used tool in laser cooling of atoms. For further details see Box 4.

BOX 4

The magneto-optical trap (MOT).

The idea of constructing a trap based on the scattering force is very appealing: by taking advantage of its dissipative nature in a set-up which also provides confinement one could construct a simple and robust trap. However, this is not straightforward. The classical Earnshaw theorem (see also Sec. V) relies on the fact that the divergence of an electric field vanishes in a charge-free region. The equivalent divergence criterion for light is that in free space, there are no sources or sinks for photons. This implies an optical Earnshaw theorem stating that a trap, in which the scattering force is only proportional to the laser intensity, will be unstable. A way around this problem is to apply some external field to alter this proportionality in a position dependent way. The most successful example is the magneto-optical trap (MOT) first demonstrated in 1987 in a collaboration between Bell Labs and MIT. The idea for the MOT, as originally conceived by Dalibard at ENS in Paris, was to use circularly polarised light for optical molasses and add a spherical quadrupole magnetic field such that as an atom moves away from the origin, the transition is Zeeman shifted into resonance with a beam which pushes it back.

Fig. B4a shows how this works in 1-D (the z-axis) for a laser resonant with a transition which drives the atom from a ground state with zero angular momentum J=0 to an excited state with one unit of angular momentum J' = 1. In a magnetic field, the excited atom (spin-1) can have three 'orientations': down, horizontal, and up, these magnetic sub-levels are denoted as $m_{J'}$=-1, 0, and +1, respectively.

.....continued.....

BOX 4 (continued)

The magnetic field is of the form $B_z(z) = bz$ so the $m_{J'} = +1$ and -1 sublevels experience Zeeman shifts linear in position. To provide cooling, the laser is tuned below resonance. The beams propagating in the ±z directions are circularly polarised with the same helicity. As they propagate in opposite directions they will drive $\Delta m = \pm 1$ transitions respectively. Based on the traditional definition of handedness of circular polarisation the two beams are of the same polarisation but in laser cooling the crucial point is how the light affects the atomic transitions. In the laser cooling literature this polarisation configuration is therefore commonly referred to as σ^+-σ^- polarisation. An atom with a positive z-coordinate sees the σ^- beam closer to resonance than the opposing σ^+ beam. The atom therefore scatters more σ^- than σ^+ photons and is pushed back towards $z = 0$. For an atom with a negative z-coordinate, the scattering of σ^+ photons is strongest, so it is also pushed back towards z=0. Thus, in addition to friction due to optical molasses, the atom also experiences a restoring force $F = -\kappa z$.

The generalisation to three-dimensions is illustrated in Fig. B4b. The magnetic field is provided by two coils with opposing currents (anti-Helmholtz coils). The first demonstration of the MOT used field gradients on the order of 5 Gauss/cm and achieved a trap with a depth of about 0.4 K. In terms of velocity this means that atoms slower than a critical velocity v_c of ~17 m/s could be trapped. Around 10^7 atoms were confined in a ~0.5 mm diameter cloud and observed to have a temperature of less than 1 mK and a lifetime of around 2 minutes.

An important development was the demonstration in 1990 by Wieman and co-workers in Boulder that the MOT can collect atoms directly from a room temperature vapour. There are enough atoms in the tail of the thermal Maxwell-Boltzmann distribution slower than v_c to provide a substantial loading rate. The convenience of this set-up has turned the MOT into an extremely useful tool and the basic building block in most experiments using laser cooled atoms.

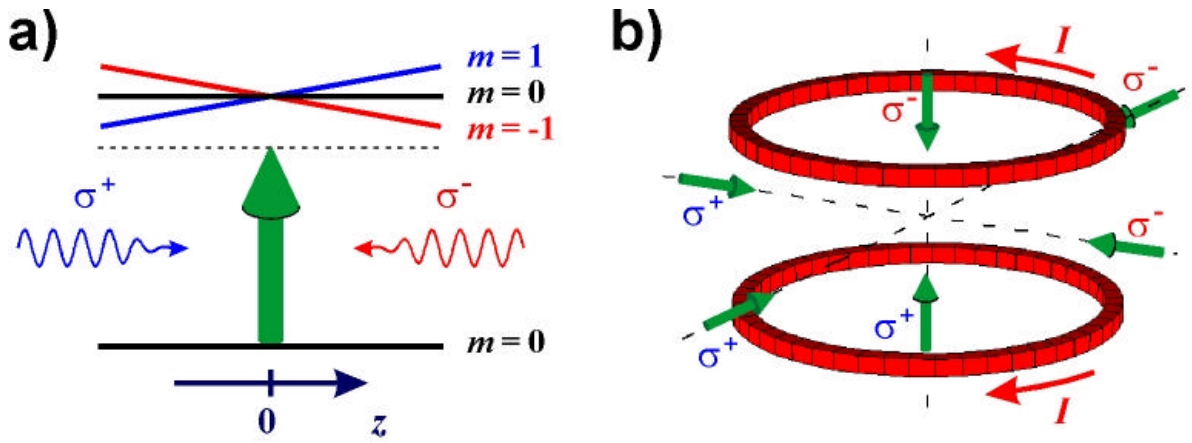

Fig. B4. *The magneto-optic trap (MOT): (a) An atom with a J = 0 to J' = 1 transition is placed in a linearly varying magnetic field $B_z(z) = b\ z$. For an atom with a positive z-coordinate, the σ^- beam, which drives the $\Delta m = -1$ transition and propagate to the right is closer to resonance, than the σ^+ beam which drives the $\Delta m = +1$ transition and propagates to the left. The net force pushes the atom towards $z = 0$; (b) The three-dimensional generalisation uses two coaxial coils with opposing currents and three orthogonal standing σ^+–σ^- waves.*

B. Sub-Doppler cooling

Although the first experiment on 3-D optical molasses appeared to be in fair agreement with the theoretical expectation, a number of mysteries soon emerged. Early quantitative measurements by the NIST group on

the properties of optical molasses yielded a number of surprising results at odds with the Doppler cooling theory. In fact, it soon became apparent that 3-D optical molasses worked significantly better than had been anticipated!

In Doppler theory, the lifetime of optical molasses is approximately equal to the time required for an atom to diffuse to the edge of the interaction region. The lifetime should be extremely sensitive to slight imbalances in the intensities of the counter-propagating beams. An imbalance of a few percent should sweep the atoms out with a velocity of several cm/s, limiting the lifetime to tens of ms. However, experiments demonstrated lifetimes on the order of 0.5 s, and hardly any change for intensity imbalances of up to 10%. Furthermore, deliberate large misalignments of the beams lead to even longer confinement times referred to as 'super molasses'. But the clearest evidence that something was terribly wrong with the theory was the careful measurement of the sodium molasses temperature by the NIST group. Their result was 43±20 μK, whereas theory predicted ~240 μK. The dependence of the temperature on detuning was also completely different than expected.

The key to understanding these discrepancies is to drop two simplifying assumptions of the Doppler cooling theory. First, the two-level nature of the atom (Na has more than a dozen levels playing an active role in the cooling process). Second, the assumption that the light field has a pure state of polarisation (at best only possible to realise in two dimensions).

Two distinct mechanisms have been identified to explain the lower than expected temperatures observed in experiments. They are associated with the two distinct types of *polarisation gradients* which arise in the interference of light beams. These may be illustrated by considering counter-propagating beams with orthogonal linear polarisations (lin⊥lin), and counter-propagating beams imposing opposite changes in the atomic angular momentum (σ^+–σ^-) (as in the MOT, see Box 4). In the former, the polarisation varies between linear and circular as shown in Fig. 7a over a distance of half a wavelength. In the latter (shown in Fig. 7b) the polarisation is linear everywhere along the beam, but the direction of the polarisation rotates forming a helix.

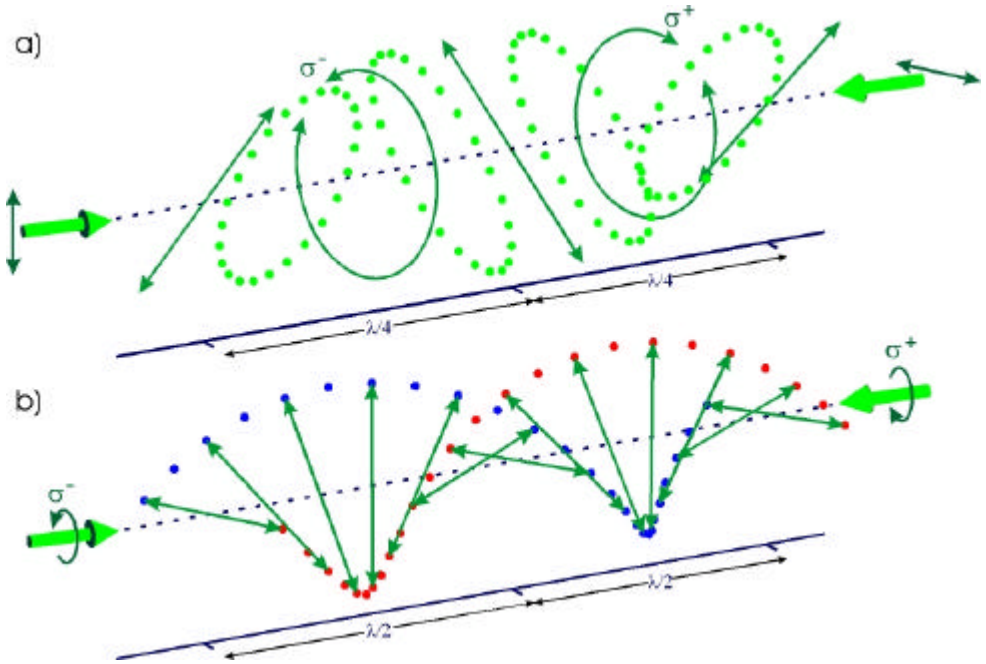

Fig. 7. *The two field configurations considered in polarisation gradient cooling: (a) The two beams are both linearly polarised, but in orthogonal directions (lin⊥lin). The polarisation of the field varies from linear through circular to the opposite linear and back again over a distance of λ/2; (b) The two beams are circularly polarised in opposite directions (σ^+–σ^-). The electric field is linearly polarised everywhere, but the direction of polarisation rotates around the propagation direction with a pitch of λ/2.*

Fig. 8 a and b show the multi-level nature of the cooling transition in Na. The transition is from a ground state with total angular momentum $F = 2$ to an excited state with total angular momentum $F' = 3$. In a magnetic field, the angular momentum vector can have $2F+1$ possible orientations, each labelled by an m_F quantum number. Indicated in the figure are the coupling strengths between the ground and excited state m_F levels for linearly and circularly polarised light. The light-shift (proportional to the coupling strength), and the steady-state populations of each levels for a stationary atom are also shown. The figure illustrates how absorption and spontaneous emission tends to transfer population to the most light-shifted level. This process is known as *optical pumping*. In this example, optical pumping is equivalent to an alignment of the atomic dipole with the field. Indeed an $F \rightarrow F+1$ transition behaves very much like a classical damped oscillator, whose motion will follow the driving field with a time delay characteristic of the relaxation process causing the damping.

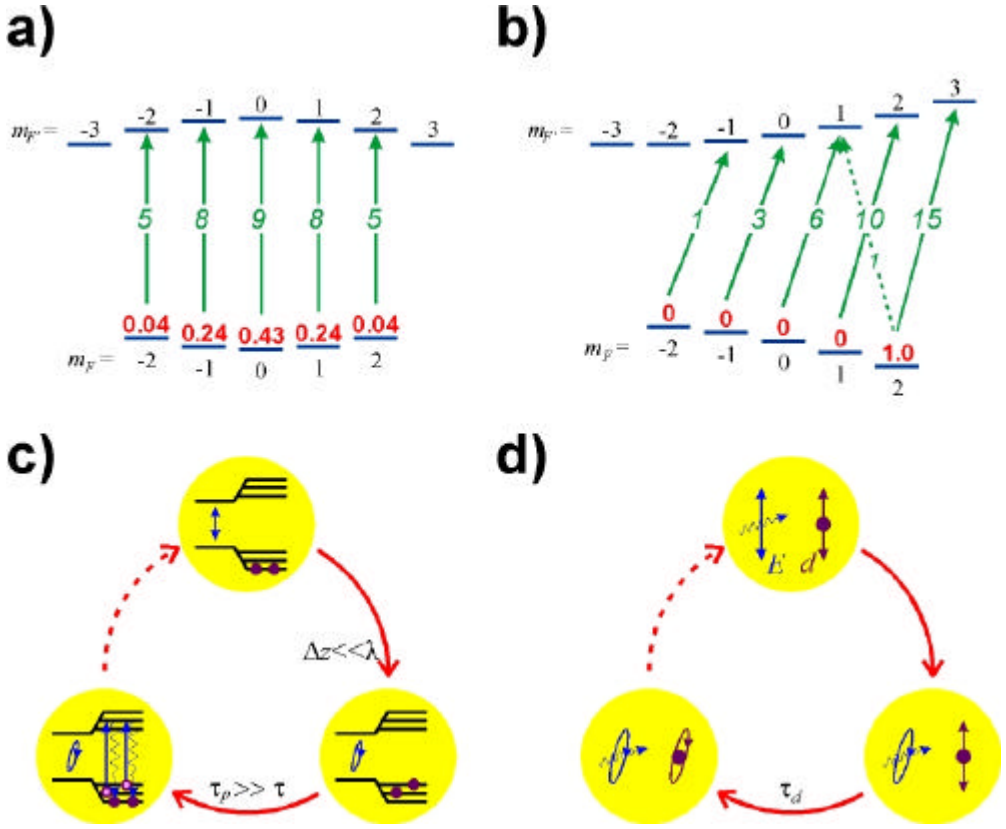

Fig. 8. *Polarisation gradient cooling of Na: The magnetic sublevels of the $3^2S_{1/2}$, F=2 to $3^2P_{3/2}$, F'=3 cooling transition for (a) linearly and (b) circularly (σ^+) polarised light. Also shown are the relative light shifts, the relative coupling strengths for the individual transitions (in green) and the steady-state populations (in red). In both cases, the atom aligns with the field, i.e. optically pumps towards the most light shifted level. (c) The cooling mechanism for lin⊥lin polarisation: The atom starts by optically pumping into the lowest energy level (top). It then moves a fraction of a wavelength to a point with elliptical polarisation, where it now is no longer in the state of lowest energy. Finally, optical pumping brings the atom back to a state of lowest energy equivalent to the initial state. The timescale τ_p is in the order of several natural lifetimes. (d) In the classical analogue of polarisation gradient cooling in lin⊥lin polarisation, the (atomic) dipole **d** has the lowest potential energy if it is aligned with the field **E**. However, it can only follow a change in the field with a finite time constant, τ_d, characteristic of the damping process. When it moves through the field, kinetic energy is transformed first to potential energy and then lost due to damping as the dipole relaxes to the new state of polarisation.*

The polarisation gradient cooling mechanism for lin⊥lin polarisation is shown schematically in Fig. 8c. Fig. 8d shows the classical analogue. Consider an atom, beginning at a position of linear polarisation (top). The atom is optically pumped predominantly into the lowest energy level, i.e., the atomic dipole is aligned with the field. If it now moves a fraction of a wavelength in less than an optical pumping time, the polarisation of the light changes to elliptical but the state of the atom does not have time to adjust. Therefore, population is transferred non-adiabatically to a superposition of levels, that on average are less strongly coupled to the light. The corresponding reduction in the light shift means that the atom has increased its internal energy at the expense of kinetic energy. This is similar to the Sisyphus effect discussed in Box 5. The atom is no longer in the state of lowest energy, or equivalently the dipole moment is no longer parallel to the electric field. Subsequently, the atom is optically pumped back into the lowest energy state, i.e. the atomic dipole realigns with the field. During this 'repumping' process, the spontaneously emitted photons have slightly more energy than the absorbed photons, so kinetic energy is extracted by the emitted light. The timescale for the optical pumping, τ_p, depends on the intensity, but is typically several natural lifetimes. This mechanism is only important for atoms moving slower than a characteristic velocity υ_c, corresponding to the atom moving a distance on the order of $\lambda/8$ in an optical pumping time.

The mechanism involved in the sub-Doppler cooling in σ^+–σ^- polarisation is somewhat different. As the electric field is everywhere linearly polarised and has constant amplitude, the Sisyphus mechanism is not active in this case. The starting point is again an atom at rest in the optically pumped state, as shown in Fig. 8a. When the atom starts to move (for instance towards the σ^+ beam) the symmetry is broken. The σ^+ beam becomes closer to resonance and the atom is optically pumped towards the positive m_F levels. This is a run-away effect because positive m_F levels couple more strongly to σ^+ light (for the $m_F = 2$ level in Na the σ^+ coupling is 15 times stronger than for σ^-, as shown in Fig 9b). This motionally induced redistribution of the population enhances the difference in the scattering rates from the two beams leading to a much stronger frictional force than would occur for a two-level atom (Doppler cooling). For atoms faster than a characteristic velocity υ_c (same order of magnitude as in the case of lin⊥lin polarisation) the redistribution of population washes out and the cooling force returns to the normal Doppler expression.

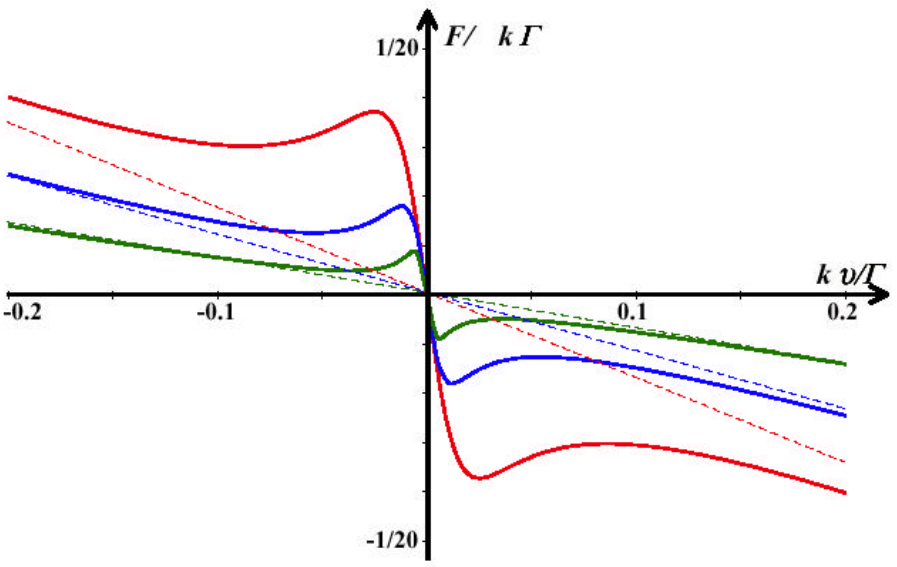

Fig. 9. *The cooling force vs. velocity for lin⊥lin polarisation. The three solid curves are for intensities equal to I_{sat} (red), $I_{sat}/2$ (blue), and $I_{sat}/4$ (green). The dashed lines are the corresponding contributions from Doppler cooling.*

The two polarisation gradient cooling mechanisms are characterised by a small capture velocity proportional to the laser intensity and a relatively large friction coefficient which, contrary to the case of Doppler cooling, is independent of intensity. This is illustrated in Fig. 9 which shows the theoretical force vs. velocity curve for lin⊥lin polarisation for three different intensities.

BOX 5

The Sisyphus effect.

It is instructive for the understanding of sub-Doppler cooling to consider briefly the motion of a two-level atom in a strong standing wave as originally described by Cohen-Tannoudji and Dalibard in Paris. Consider an atom in a strong ($\omega_R >> \Delta$) laser field tuned above resonance ($\Delta > 0$). The dressed atom picture, Fig. B5, looks very similar to the one shown for $\Delta < 0$ in Fig. B3b, except that the ground and excited state labels (g and e) are interchanged and the dressed state energies vary sinusoidally with position. Just as important for the arguments to follow, the atomic state changes from a pure state ($|e,n\rangle$ or $|g,n+1\rangle$) at the nodes of the field, to superpositions of these states at the anti-nodes (cf. Box 3).

The mechanical effect of light can be understood by following the trajectory of an atom through the dressed atom potentials and including the dissipative effect of spontaneous emission as a transition between manifolds. Consider an atom that starts in the ground state near a field node (for instance with n+2 photons in the field). If it moves slowly ($kv << \omega_R$) it will remain in the dressed state $|1(n+1)\rangle$ until disturbed by spontaneous emission. As the atom moves away from the field node the increase in internal energy results in a decrease in kinetic energy, i.e. the atom is slowed down. As the atom climbs up the hill towards the anti-node, the wavefunction takes on more and more of the character of the excited state ($|e,n+1\rangle$) and the probability of spontaneous emission increases. The atom can decay either to the equivalent state one step further down the ladder ($|1(n)\rangle$), which from a mechanical point of view is insignificant, or to the $|2(n)\rangle$ level, in which case it would find itself back near the bottom of a potential valley. Thereafter the process repeats, i.e., the atom climbs up the next hill, the excited state component and hence the probability of spontaneous decay again increase towards a maximum at the field node, where the atom is likely to decay to a valley in the $|1(n-1)\rangle$ potential. Thus, the atom spends most of its time climbing hills, thereby converting kinetic energy into light. This cooling mechanism is generally referred to as '*Sisyphus cooling*', due to the similarity with the Greek myth about Sisyphus.

The situation described above provides cooling for a laser field tuned above resonance (blue detuning), contrary to Doppler cooling. The mechanism only works for slow atoms; those moving less than a quarter of a wavelength in a natural lifetime. A similar mechanism involving multi-level atoms is active in red detuned lin⊥lin polarisation gradient cooling, as described in the main text.

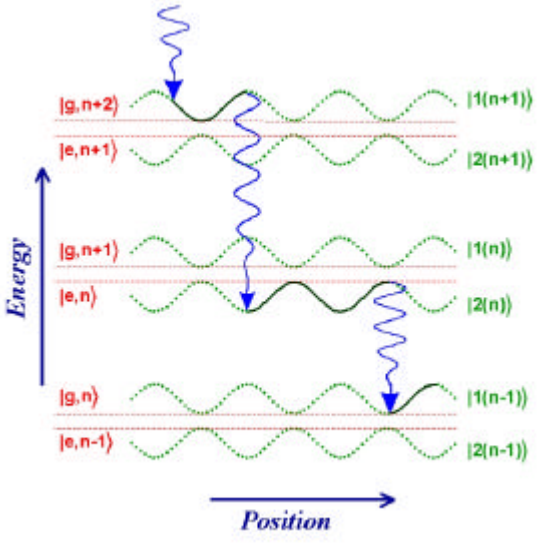

Fig. B5. *Sisyphus cooling of an atom in a standing wave: Near the nodes of the field, the energies are unshifted and the dressed wave functions coincide with the atomic wave functions, while near the anti-nodes, the wave functions are mixed. Spontaneous emission occurs preferentially where the dressed state has most excited state character, i.e., from the anti-nodes of states* $|1(n)\rangle$ *and the nodes of states* $|2(n)\rangle$*. The solid curve represents the motion of a slow atom through the standing wave. The net effect of spontaneous emission is such that the atom travels uphill more than downhill.*

Extensive experimental investigation of sub-Doppler cooling has been carried out both in 1-D and 3-D. The lowest temperature of 2.5 μK was obtained for 3-D optical molasses in Cs (compare to the Doppler limit of 120 μK). This corresponds to an r.m.s. momentum of ~3.5 $\hbar k$ in each direction. A further careful investigation of this system was carried out in Paris, and it was found that the temperature for a sufficiently large detuning ($|\Delta| > 5\Gamma$) was linear in the parameter I/Δ, which is simply the depth of the valleys in the Sysiphus mechanism (see Box 5). This dependence and the minimum velocity spread of a few recoil velocities are predicted by the complete theoretical analysis of polarisation gradient cooling.

C. Sub-recoil cooling

In Sec. IV B we saw that, for multi-level atoms, the fundamental laser cooling limit is characterised by an r.m.s. velocity $\upsilon_{rec} = \hbar k/m$ or a recoil temperature defined by $T_{rec} = \hbar^2 k^2 / m k_B$. A way around the recoil limit is to rely on the stochastic nature of spontaneous emission to kick atoms into a select region of velocity space, with dimension less than υ_{rec}, where the scattering rate drops to zero (see Fig. 10). This idea is sometimes referred to as velocity space optical pumping, and the excitation free region around $\upsilon = 0$ can be referred to as a dark state or dark region. In principle, there is no minimum temperature, but as the process relies on a random walk it takes longer and longer to reach lower temperatures.

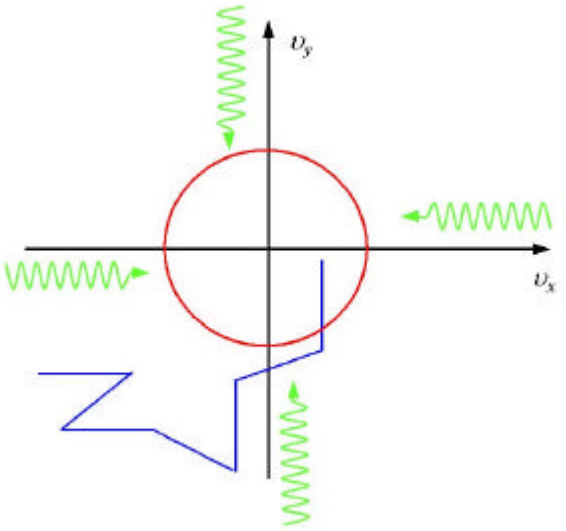

Fig. 10. *The principle of sub-recoil cooling explained in terms of velocity space optical pumping. During cycles of absorption and emission of light the atoms undergo a random walk in velocity space (indicated by the blue line). As for Doppler cooling the velocity steps during the excitation part of the cycle are weighted towards $\upsilon = 0$ due to the Doppler effect. If one arranges that when the atom falls within a recoil velocity υ_{rec} of $\upsilon = 0$ (indicated by the red circle), no further excitation occurs then atoms will accumulate with $\upsilon < \upsilon_{rec}$.*

Sub-recoil cooling requires high velocity selectivity around $\upsilon = 0$, but should still address any atoms with $\upsilon > \upsilon_{rec}$. This is the inverse of the usual excitation spectrum: a narrow linewidth transition excites only those atoms within a narrow velocity range, whereas for sub-recoil cooling the goal is to excite all atoms except those within a narrow velocity range. The two most successful sub-recoil schemes achieve this goal in very different ways. In velocity selective coherent population trapping (VSCPT), atoms close to $\upsilon = 0$ are decoupled from the light due to destructive interference between two terms that contribute to the excitation rate. In stimulated Raman cooling, a narrow linewidth transition is tuned through the velocity distribution to actively remove atoms from the wrong velocity classes, and guide them towards $\upsilon = 0$.

Both sub-recoil schemes may be used to cool in any number of dimensions. However, as they both rely on momentum diffusion, the cooling time scales rapidly with the dimensionality: in 1-D, the random walk must find a slab in velocity space, in 2-D a cylinder, and in 3-D a sphere. Also, in a 1-D or 2-D random walk all the paths pass through the origin eventually, whereas in 3-D some never do. For this reason efficient 3-D cooling relies on the assistance of the Doppler effect to direct them towards zero velocity. Fig. 11 illustrates the advantage of adding Doppler selectivity to the random walk process.

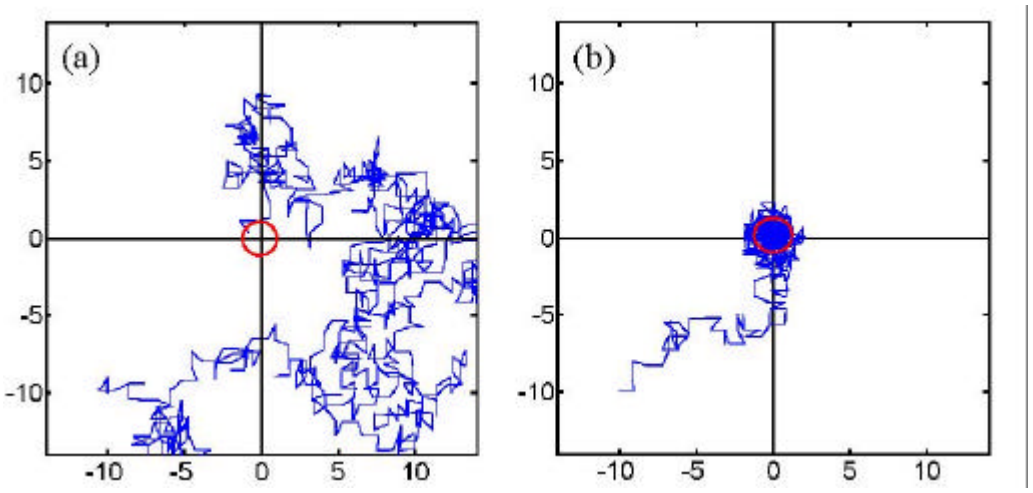

Fig. 11. *Schematic illustration of 2-D random walk trajectories for (a) VSCPT and (b) Raman cooling: (a) In VSCPT all atoms are cooled simultaneously but as photons are absorbed from both directions with almost equal probability it can take some time for them to find their way to* $\upsilon = 0$. *When they do the scattering rate drops and they remains there essentially indefinitely; (b) Raman cooling uses extremely sensitive velocity selectivity to select atoms with a given initial velocity and sequentially push them towards* $\upsilon = 0$. *In this case, the time is consumed in working through all the initial velocity classes.*

1) Velocity selective coherent population trapping (VSCPT)

Velocity selective coherent population trapping (VSCPT) is based on momentum diffusion into a dark state (see Box 6): The atoms scatters light until diffusion brings them towards zero velocity where the scattering slows, stopping completely at $\upsilon = 0$. If the velocity is not quite zero, scattering can still occur and diffusion has another chance to push the atom closer to $\upsilon = 0$. The process acts as a 'velocity trap' leading to the accumulation of atoms near $\upsilon = 0$, hence the term velocity selective population trapping. In the standard VSCPT scheme, the dark state is a superposition of two grounds states, both with one photon recoil of momentum but in opposite directions ($|g_-,-\hbar k\rangle$ and $|g_+,+\hbar k\rangle$, see Box 6), so the momentum distribution tends towards two narrow peaks at $\pm\hbar k$. The width of the peaks is proportional to $1/\sqrt{T}$, where T is the interaction time. The first experiment on VSCPT was performed on a metastable helium atomic beam by Aspect *et al*. in 1988. They observed the characteristic double-peaked distribution with a peak width equivalent to an r.m.s. velocity, $\upsilon_{rms} = 0.65\ \hbar k/m$. This width was mainly limited by the interaction time. In 1994 this time was increased by an order of magnitude using laser cooled helium atoms giving $\upsilon_{rms} = 0.2\ \hbar k/m$.

VSCPT can be extended to 2 and 3 dimensions. In 2-D, two orthogonal counter-propagating beam pairs are used, resulting in four wavepackets with momenta $\pm\hbar k_x$, and $\pm\hbar k_y$ as shown in Fig. 12. Similarly, in 3-D, six wavepackets are produced. However, this need not be a drawback as the entire population of the dark state can be transferred to a single momentum state by adiabatically lowering the intensity of all but one of the laser beams.

The physics underlying the stochastic filling of the dark state has some interesting parallels with other complex systems. If one considers the dark region as a trap, the dynamics of an atom can be modelled as a sequence of trapping times interspersed with escape times. As the probability for escape falls to zero at $\upsilon = 0$ there is finite probability of extremely long trapping times. Consequently the distribution of trapping times is Lorentzian, i.e., long tailed. In contrast, for a simple random walk the distribution is Gaussian, and the probability of large excursions from the mean are extremely small. The Lorentzian distribution is characteristic of process described by Lévy flight statistics. Other examples include the foraging of an albatross and pinball.

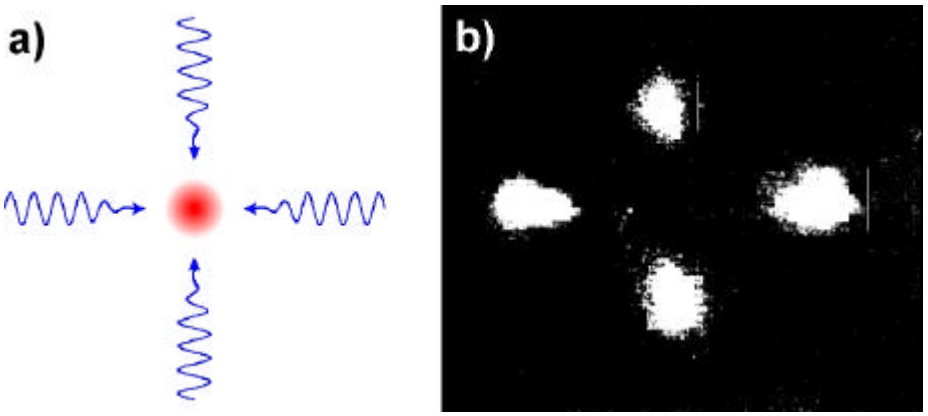

Fig. 12. *VSCPT in 2-D: (a) Experimental set-up for 2-D velocity selective coherent population trapping. The interaction region consists of two orthogonal* σ^+–σ^- *light fields; (b) The dark state is of a superposition of four momentum states,* $\pm\hbar k_x$ *, and* $\pm\hbar k_y$ *, leading to the atomic distribution shown. The r.m.s. velocity width of the peaks was* $0.25\hbar k/m$ *. (Figure courtesy of C. Cohen-Tannoudji).*

2) Raman cooling

In Raman cooling, a two-photon transition between two levels in the ground state is used to select a narrow velocity class and actively push it towards zero velocity. As both the initial and final levels are ground states, the transition linewidth is inversely proportional to the interaction time and can be extremely narrow, allowing narrow velocity classes to be addressed. The transition is driven by applying two laser beams whose frequency difference is equal to the ground state splitting. If both beams are far-detuned from the single-photon resonance, the probability for off-resonant excitation of the optical transition is small, and the excited state can be neglected.

For an atom with velocity υ, the Raman resonance condition is,

$$\omega_1 - \omega_2 = \left(k_1 - k_2\right)\cdot\upsilon + \Delta_{gs}$$

where $\omega_{1,2}$, $k_{1,2}$ are the frequencies and wavevectors of the laser beams, and Δ_{gs} is the ground state splitting. For co-propagating beams $k_1 = k_2$ and the Doppler shifts cancel (this is the Doppler-free configuration traditionally used in Raman spectroscopy). For counter-propagating beams $k_1 = -k_2$, the Doppler shifts add and the transition remains Doppler sensitive. In this velocity sensitive configuration, the Raman beams can be tuned to address a particular velocity class, with a width determined by the duration of the Raman pulse.

The Raman cooling cycle is depicted schematically in Fig. 13. If initially the Raman beams are detuned to the red of the Raman resonance they interact with atoms in the lower hyperfine level with velocity around $\upsilon = -3\hbar k/m$, Fig. 13a. These atoms are transferred to the upper level, while their velocity is increased by $2\hbar k/m$, Fig. 13b. The atoms are returned to the lower level by an optical pumping pulse resonant with the single photon transition, Fig. 13c. On average this results in a velocity change of $\hbar k/m$ so the net result of the sequence is to select atoms with $\upsilon = -3\hbar k/m$ and deposit them around $\upsilon = 0$. By reversing the direction of the Raman and the optical pumping beams, atoms with the opposite velocity are selected. Thus, a sequence of Raman pulses with various detunings and directions can be used to push all the atoms towards $\upsilon = 0$.

BOX 6

Dark states and coherent population trapping

To understand the principle of dark states and coherent population trapping, consider an atom where both the ground and excited state of the cooling transition have one unit of angular momentum, i.e., J=1 and J'=1 respectively. In a magnetic field a spin-1 can have three 'orientations': down, horizontal, and up, which are denoted as m_J=-1, 0, and +1, respectively. We label the three ground and excited magnetic sub-levels as $|g_-\rangle$, $|g_0\rangle$, $|g_+\rangle$ and $|e_-\rangle$, $|e_0\rangle$, $|e_+\rangle$ (see Fig. B6). Now consider the atom in a light field formed by orthogonal circularly polarised laser beams (σ^+–σ^-) propagating in the ±z-directions, respectively, as in Fig. 7b. The $\sigma^\pm$ photons drive transitions from a groundstate sub-level m_J where the atom has momentum p, to an excited state sublevel $m_{J'} = m_J \pm 1$ with momentum $p' = p \pm 1$. Consequently the magnetic sub-levels can be divided into two families: $\{|e_-, p-\hbar k\rangle, |g_0, p\rangle, |e_+, p+\hbar k\rangle\}$ which form a V-system, and $\{|g_-, p-\hbar k\rangle, |e_0, p\rangle, |g_+, p+\hbar k\rangle\}$ which form a Λ-system. The two families are coupled by spontaneous emission. However, this is a one way process: there is no decay route from Λ to V because $m_{J'} = 0$ to $m_J = 0$ is not allowed in a J = 1 to J' =1 transition. Therefore, after a few cycles, all the atoms are pumped into the Λ-system, and we can neglect the V-system.

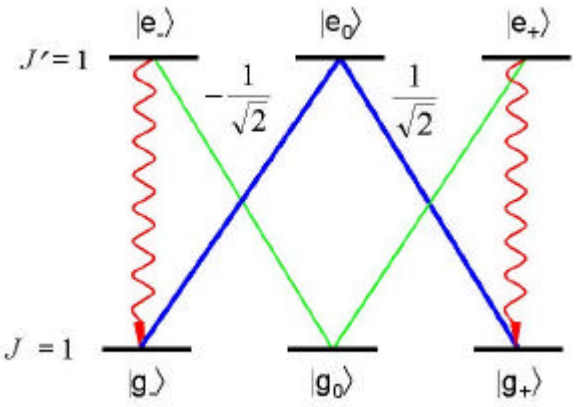

Fig. B6. *The level scheme for a J=1 to J'=1 transition in a σ^+–σ^- light field.*

In the Λ-system, the atom can decay into $|g_-, p-\hbar k\rangle$, $|g_+, p+\hbar k\rangle$ or a superposition, $|g_-, p-\hbar k\rangle \pm |g_+, p+\hbar k\rangle$. A superposition of magnetic sub-levels is somewhat analogous to a superposition of light. Just as the σ^+–σ^- light field forms a helix, (Fig. 7b), the atomic dipole moment $\boldsymbol{d}$, between the $|g_-, p-\hbar k\rangle + |g_+, p+\hbar k\rangle$ and the excited state $|e_0, p\rangle$ is also helical, with the same pitch as the electric field $\boldsymbol{E}$. However, for a stationary atom the dipole helix is π/2 out-of-phase with the electric such that the $\boldsymbol{d}$ and $\boldsymbol{E}$ are everywhere orthogonal, therefore, the transition probability (proportional to $-\boldsymbol{d}\cdot\boldsymbol{E}$) is zero, i.e., the state is completely uncoupled from the light. Thus, once the atom finds itself in this superposition of $|g_-, -\hbar k\rangle$ and $|g_+, \hbar k\rangle$, it will remain there indefinitely. This is referred to as coherent population trapping and the non-coupled state is known as a dark state. The dark state only exist for a stationary atom: if the atom is moving the phase between the atomic dipole and electric field changes and the average transition probability is no longer zero.

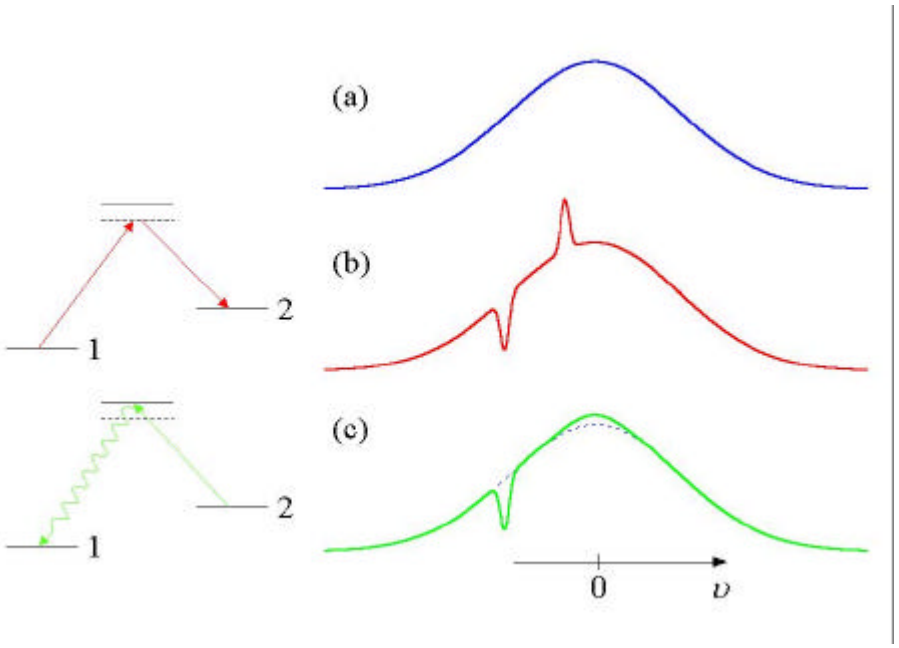

Fig. 13. *Raman cooling: (a) the initial velocity distribution in the lower ground state (1). The Raman laser beams are tuned to resonance with a group of atoms with a particular velocity. They are transferred to the upper ground state (2) and have their velocity increased by* $2\hbar k/m$ *as shown in (b). The atoms are returned to the lower ground state by a pulse of light on a single photon transition followed by a spontaneous emission. This results in a further increase of the velocity by* $\hbar k/m$ *and a broadening as shown in (c). The net effect is that the initial group of atoms on average has been slowed down by* $3\hbar k/m$ *.*

The Raman cooling scheme described above was conceived and demonstrated by Kasevich and Chu at Stanford in 1992. In the experiment the r.m.s. velocity width of Na atoms, released from optical molasses, was reduced from 4 to 0.2 $\hbar k/m$ (see Fig. 14). Raman cooling can be extended to two and three dimensions, but becomes rather beam 'intensive'. It also works well on atoms in a far-off resonance optical dipole trap (see Sec. V B), which has the advantage that only one Raman beam pair is required to cool all three dimensions. In tightly bound traps, one may adapt the scheme to perform Raman sideband cooling (see Sec. V D).

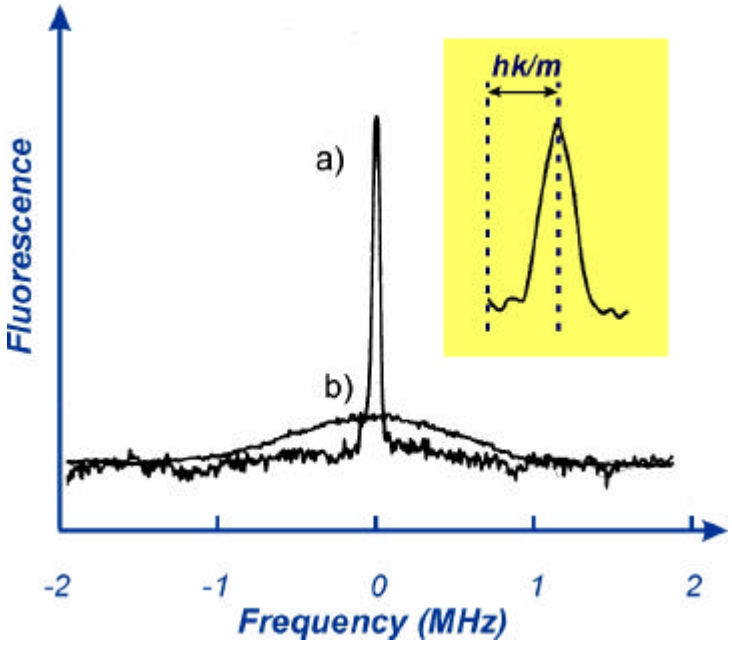

Fig. 14. *a) The velocity distribution after 5.7 ms of Raman cooling. The velocity distribution was measured by scanning the frequency of a stimulated Raman detection pulse. Inset, an enlarged view of the central peak illustrating the velocity width relative to the photon recoil velocity. The initial velocity distribution is shown as b). (Figure courtesy of S. Chu).*

V. TRAPPING OF NEUTRAL PARTICLES

Trapping particles is not as straightforward as it may seem. Earnshaw's theorem states that it is impossible to create a potential minimum, or trap, based on static fields only. The force is equal to the gradient of a potential, and the divergence of a gradient is zero, therefore, the field lines cannot converge on a point where the net force is zero. In fact, most 'traps' are based on dynamical forces associated with motion of electrons within atoms. Alternatively, dynamical trapping forces may be introduced by applying time-varying fields. A good example is the Paul trap used for confining ions, where an alternating electric field is applied to a configuration of electrodes consisting of a ring and two end caps. Depending on the polarity of an applied field, the central point is either axially stable and radially unstable or vice versa, in accordance with Earnshaw's theorem. By alternating the polarity faster than the natural oscillation frequency of the system (in this case nearly zero), this point becomes *dynamically stable*. Balancing a pencil on a finger tip by rapidly moving the finger is a kind of mechanical analogue of the Paul trap.

Optical trapping of neutral particles is also analogous to the Paul trap. In this case, the oscillating electric field is provided by a laser. If the laser is tuned below any resonances of the system (red detuning), the particle is dynamically stable at the position of maximum field. This is opposite to the Paul trap where the driving frequency is above resonance (blue detuning), and the dynamical force attracts the ion to the centre where the field vanishes.

In principle, neutral atoms may be trapped by light forces or using static electric or magnetic fields. However, in practice, an optical version of Earnshaw's theorem precludes trapping by radiation pressure alone (see also Box 4), and the interaction with electric and magnetic fields is so weak that atoms must be pre-cooled to very low temperatures to be trapped. Before laser cooling, this pre-cooling has to be performed with liquid helium and only hydrogen had been successfully trapped. Laser cooling has made it possible to trap a great variety of atomic species. The two main types of neutral atom traps are based on magnetic fields and the optical dipole force.

A. Magnetic trapping of atoms

The principle of a magnetic trap is similar to the Stern-Gerlach effect, i.e., the force on a magnetic dipole in a magnetic field gradient. An atom with a magnetic dipole moment $\vec{\mu}$, in the presence of a magnetic field $\vec{B}$, has a potential energy $-\vec{\mu}\cdot\vec{B}$. If the magnetic field is non-uniform, it exerts a force $\mu\nabla B$. The atom is attracted to low- or high-field depending on whether $\vec{\mu}$, is parallel or anti-parallel to $\vec{B}$. However, in practice, it is impossible to create a local maximum of a magnetic field, so only low-field seekers can be trapped.

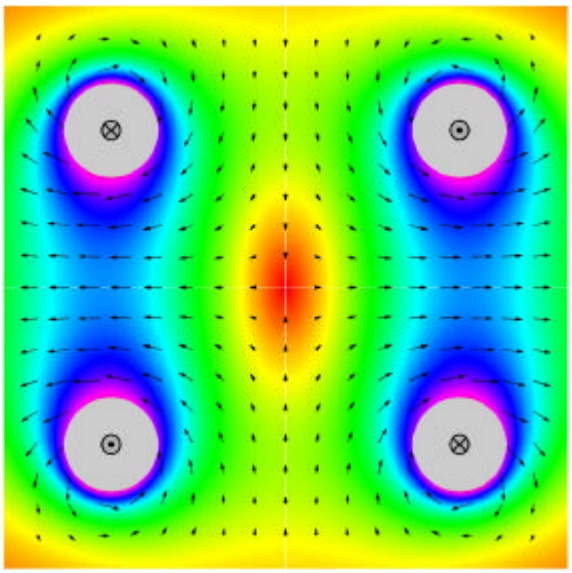

Fig. 15*. Magnetic trapping can take place in the zero-point of the magnetic field created by two current loops (grey, out of the plane of the paper) in the anti-Helmholtz coil configuration. The colours indicate the magnitude of the magnetic field with red corresponding to B = 0. The arrows indicate the direction and magnitude of the field.*

Magnetic traps provide a conservative potential ideally suited for confining atoms prepared by laser cooling. Compared to optical dipole traps (see next Sec.) the trapping potential is relatively deep: for Na atoms, a field variation of only 15 Gauss corresponds to a trap depth of 1 mK. However, the field gradient required is still one or two orders of magnitude larger than used in the magneto-optical trap (see Box 4) (a field gradient of 15 Gauss/cm is required to support rubidium against gravity).

Early magnetic traps used an anti-Helmholtz coil configuration producing a spherical quadrupole field. The field contours are shown in Fig. 15. The atoms are optically pumped into a spin-up level and as long as they stay clear of the zero-field point, their spin follows the local magnetic field, resulting in a trapping potential determined solely by the field magnitude.

In general for magnetic coils of radius R, producing a magnetic field B, the trapping potential scales as,

$$U(r) \sim \mu B\left(r/R\right)^n$$

for $r << R$, where n depends on the coil configuration. The anti-Helmholtz trap is linear, $n = 1$, producing the strongest confinement; ideal for achieving high density. However, linear traps are inherently leaky because the field is zero at the origin: an atom passing near the origin, experiences a rapid change in the sign of the field which the atomic spin cannot follow, the atom finds itself in an anti-trapped state and is ejected. This loss mechanism, known as a Majorana spin flip, is disastrous for cooling because colder atoms spend more time in the vicinity of zero field, and become more likely to flip. Techniques to eliminate this problem were first developed in 1995 at JILA by adding an oscillatory magnetic field to rotate the zero-field position such that the effective potential appears parabolic, see Fig. 16; and at MIT using a far-blue-detuned laser beam to prevent atoms entering the zero-field region. However, when steps are taken to reduce the spin-flip loss some of the advantages of tighter confinement are lost.

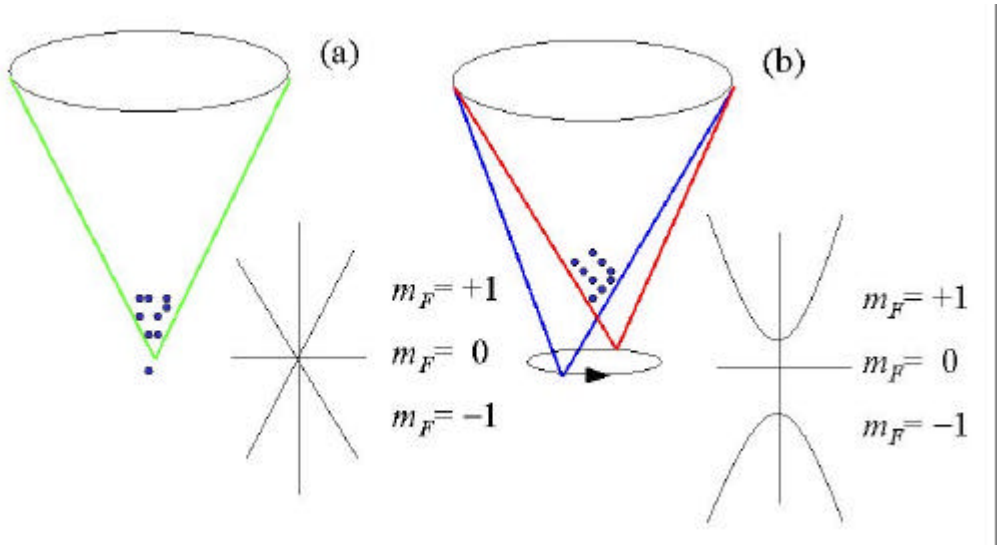

Fig. 16. *(a) The linear magnetic trap showing the lossy zero-point of the magnetic field. (b) The TOP trap: An oscillatory magnetic field is applied to rotate the zero-field position. If the rotation period is much faster than the oscillation period of trapped atoms, the time-orbiting potential (TOP) is parabolic with no zero-crossing, so the spin-flip loss rate is significantly reduced.*

Alternatively, one may construct a trap with non-zero field at the origin, in which case, the trapping potential is parabolic, n=2, resulting in weaker confinement. The standard parabolic trap, known as Ioffe-Prichard, consists of four straight conductors in quadrupole configuration with two coils for end caps. There are many variations on this theme whose names often reflect their respective geometies, e.g., the baseball trap, where the windings follow the pattern of stitching on a baseball.

B. Optical dipole traps

Similar to the magnetic trap where a magnetic dipole is confined by a magnetic field gradient, the optical dipole trap confines an electric dipole $\vec{d}$ in the gradient of an electric field $\vec{E}$. However, an important difference is that the electric dipole moment is induced by an oscillatory electromagnetic field. The atom behaves as a driven oscillator and just like a mass on a spring, if it is driven below resonance (red detuning) it oscillates in phase ($\vec{d}$ parallel to $\vec{E}$), whereas if it is driven above resonance (blue detuning) it oscillates out-of-phase ($\vec{d}$ anti-parallel to $\vec{E}$). The interaction energy is $U = -\vec{d} \cdot \vec{E}$, so for red detuning the atom is attracted towards high intensity, whereas for blue detuning atoms are repelled from high intensity (see also Box 2).

The simplest form of an optical dipole trap is a single focused Gaussian laser beam detuned to the red of the atomic resonance. The trapping potential is illustrated in Fig. 17. For experimentally realisable conditions, the trapping potential is rather shallow. For a 100 mW laser beam focused to a 10 micron waist and detuned 5 nm from the Na D-lines, the trap depth is equivalent to a temperature of 0.5 mK, so optical trapping of atoms had to wait until the invention of laser cooling!

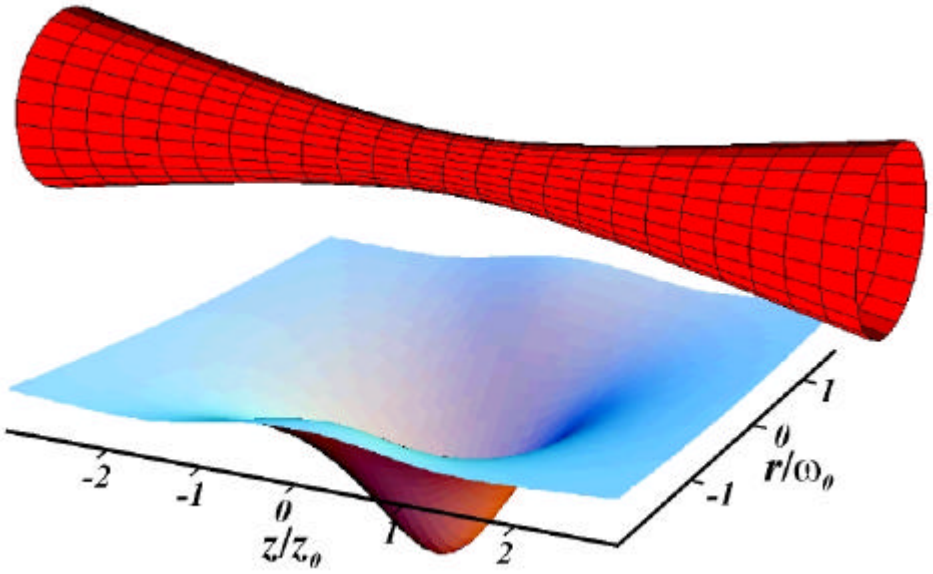

Fig. 17. *The optical dipole trap: The potential energy of an atom is lowered in the presence of a strong light field tuned below resonance.*

In fact, the first optical trap was reported only one year after the first 3-D laser cooling experiment. The trap was produced by focusing a dye laser at the centre of a Na optical molasses. To achieve sufficient trap depth, the trapping laser had to be tuned relatively close to the atomic transition. For small detunings, spontaneous scattering (1000 photons/s in this case) results in significant heating. When this was not compensated by cooling from the optical molasses beams, the trap lifetime was only a few milliseconds. However, there is a way around this problem. The trap depth is proportional to the laser power divided by the detuning, whereas the spontaneous scattering rate is proportional to the laser power divided by the *square* of the detuning. Therefore, by increasing both the intensity and the detuning one can maintain the trap depth and reduce the radiative heating. In the limit of far detuning, one expects the light to create an almost conservative potential, such that in practice the lifetime is only limited by background pressure.

Another advantage of the far-off resonance optical dipole trap is that all the groundstate magnetic sub-levels experience the same trapping potential allowing arbitrary spin states to be trapped (see Sec. IV B). Since the first optical dipole trap was demonstrated there has been a trend towards larger and larger detunings, e.g. in 1994 the Stanford group trapped Na (resonance 589 nm) using a Nd:YAG laser (wavelength 1064 nm), and in 1997 researchers in Germany and Japan trapped Cs (852 nm) using a CO_2 laser (10.6

microns). Cs atoms have also been trapped using the magnetic dipole force produced by a microwave field by the NIST group in 1994.

Another way to reduce the spontaneous scattering rate is to use blue-detuned light where atoms are repelled from regions of high intensity. The light-atom interaction time can be minimised by creating a hard-wall potential (the same principle applies to light based atom mirrors (see Chapter by Pfau and Mlynek). For example, a sodium atom cooled to the recoil temperature bouncing on an argon-ion laser beam (10 μm waist) scatters only one photon every few hours. One way to produce a hard-wall potential is to use evanescent waves. In 1993 the group at the ENS in Paris observed up to 8 bounces from a curved evanescent wave (see Fig. 18).

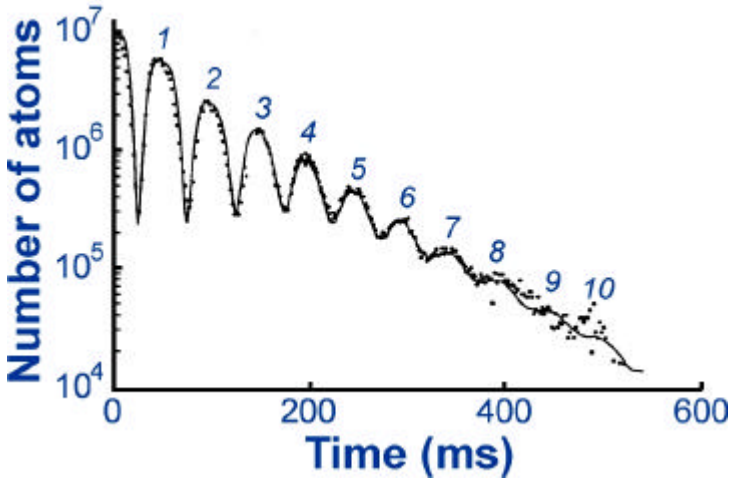

Fig. 18. *The fluorescence produced by caesium atoms bouncing on a curved evanescent wave. (Figure courtesy of C. Cohen-Tannoudji).*

A hard-wall potential can also be realised using free propagating sheets of light. The first light-sheet trap was demonstrated at Stanford in 1994. As the atoms spend most of their time in free fall, the perturbation by the light field is minimal which makes this type of trap a good candidate for spectroscopy.

C. Optical lattices

A standing wave laser field produces a periodic potential (as in Fig. B5), which can trap atoms in an ordered crystal-like structure. These crystals bound by light are known as optical lattices. A contour plot illustrating the potential wells in a 2-D lattice is shown in Fig. 19. The lattices are loaded with cold atoms prepared by optical molasses. The site occupancy is typically only a few percent, so inter-atomic interactions are almost negligible. The lattice constant, lattice type, and well depth can be chosen by selecting the geometry, polarisation, and intensity of the laser beams.

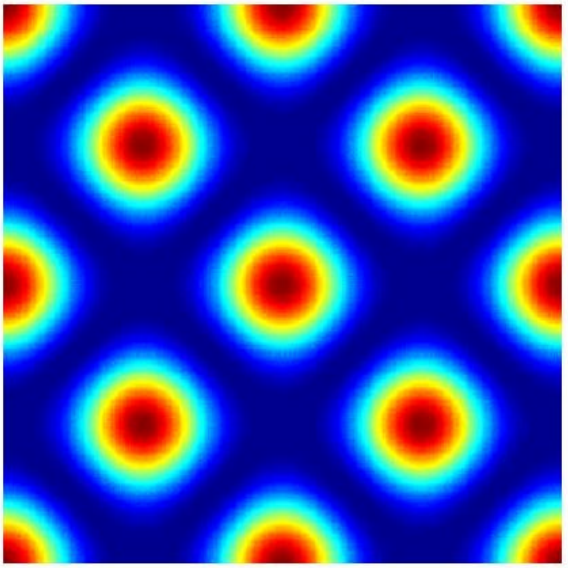

Fig. 19. *2-D optical lattice potential: Contour plot showing the optical potential produced by the intersection of two standing wave laser fields propagating along the x and y axes, and linearly polarised along the z axis.*

For near-resonant lattices ($\Delta \sim -10\Gamma$) optical pumping ensures that despite a possibly complex energy level structure the atom behaves like a harmonically bound 2-level system. A characteristic fluorescence spectrum is shown in Fig. 20. The spectrum can be explained semi-classically by considering the light scattered by an atom undergoing oscillatory motion. For a stationary atom, the scattered light has exactly the same frequency as the laser, but when the atom moves, the scattered light acquires a Doppler shift. For an atom undergoing harmonic motion the frequency of the fluorescence varies sinusoidally, so the associated electric field can be expressed as

$$E = E_0 \cos\left(\omega_0 t - ka \sin\left(\omega_t t\right)\right)$$

where ω_t and a are the frequency and amplitude of the atomic motion, and $k = 2\pi/\lambda$ is the wavevector of the trapping light. If the atomic centre of mass motion is well-localised on the scale of an optical wavelength, $ka << 1$, this can be expressed as a sum of three terms:

$$E \approx E_0 \cos\left(\omega_0 t\right) + E_0\, ka/2\left[\cos\left(\left(\omega_0 + \omega_t\right)t\right) - \cos\left(\left(\omega_0 - \omega_t\right)t\right)\right]$$

i.e., the spectrum acquires sidebands at the oscillation frequency. The ratio of sideband-to-carrier amplitude is approximately $ka/2$, which is known as the Lamb-Dicke factor. The sidebands may also be interpreted as atoms making transitions between vibrational levels of the optical potential (see Fig. 20).

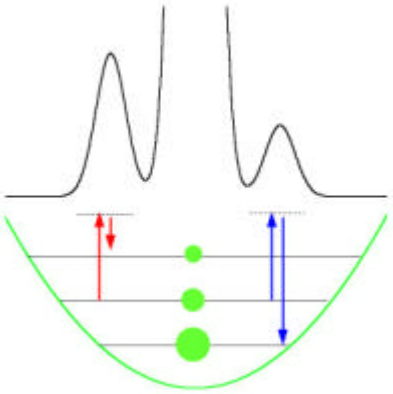

Fig. 20. *The fluorescence spectrum produced by atoms confined in a 1-D optical lattice. The lower and upper sidebands correspond to transitions up and down the vibrational ladder as indicated below.*

The asymmetry between the intensity of the red and blue sidebands reflects the thermal distribution of atoms among the vibrational levels. Assuming a Boltzmann distribution the ratio of populations in the n^{th} and $(n+1)^{th}$ levels is $\exp\left(-\hbar\omega_t / k_B T\right)$. Thus, a measurement of the asymmetry and the oscillation frequency is sufficient to determine the temperature of trapped atoms. The width of the sidebands is determined by the lifetime of the vibrational states, and is typically a few kHz for Cs.

There is considerable interest in achieving higher densities and hence higher occupancy in optical lattices. The present limits are imposed by the loading technique (typically from a magneto-optical trap) and the lattice itself. During loading and trapping, the atomic density is limited by the presence of near-resonant light. A way forward is offered by far-off resonant lattices where the cooling is provided by separate beams. Another idea is to trap atoms in a state which does not couple to the light, i.e. a dark state, similar to that discussed in the context of sub-recoil cooling (Box 6). In these dark or grey lattices, the usual light-induced density-limiting processes are reduced, allowing higher density and sometimes lower temperatures too.

The advances in preparing high density atomic samples using magnetic traps and evaporative cooling (see Sec. VI B) creates the prospect of far-off resonant optical lattices with close to 100% occupancy. In this regime the interactions between atoms become important and one would expect to observe long range cooperative ordering. Spectroscopic techniques such as Bragg diffraction can be used to detect long range order. The similarity between optical lattices and systems encountered in condensed matter physics suggests that they may offer new insight beyond the realm of laser cooling and trapping.

D. Cooling atoms in traps.

1) Laser cooling.

Laser cooling of atoms in a trap is typically very different to cooling in free space. First, the trapping fields drastically perturb the energy level structure, so, for example, the sub-Doppler cooling mechanisms described in Sec. IV B are no longer effective in a magnetic trap. Second, the character of the cooling mechanism depends on how far the atom moves during the cooling cycle. If the atoms makes many round-trips during one cooling cycle then a sideband cooling picture is appropriate. This regime is typical for ion traps and optical lattices. The opposite case, where atoms complete many cooling cycles before making one round-trip, approaches the free space cooling limit.

As atom traps are usually loaded with laser cooled atoms, we are only interested in cooling techniques that work below the usual Doppler or sub-Doppler temperatures. The simplest idea is to continue cooling on another much narrower transition: remember that the Doppler temperature is proportional to the linewidth of the atomic transition. Narrow linewidth transitions are often used for sideband cooling of trapped ions. Some atoms also have a convenient narrow linewidth transitions (e.g. magnesium and calcium) but for other reasons are not as easy to work with as the alkalis. For the alkalis, one can realise a narrow linewidth transition by driving a two-photon Raman transition between the two groundstate levels, i.e., use Raman cooling (see Sec. IV C).

Raman cooling works particularly well in far-off resonant optical dipole traps because the groundstate energy levels all experience roughly the same light shift, therefore the stimulated Raman transitions are resonant at every point in the trap. One advantage of cooling in a trap is that an anharmonic potential couples the translational degrees of freedom, such that cooling along one axis is sufficient to cool all three dimensions. In 1996 the Stanford group Raman cooled atoms in inverted pyramid optical dipole trap to a final temperature of 0.4 T_{rec}.

Raman cooling can also work in the sideband regime, as first demonstrated on trapped ions by Wineland's group at NIST and on atoms in a far-detuned optical lattice by Jessen and co-workers in Arizona in 1998. In sideband cooling, the laser is tuned to the red sideband (on the left in Fig. 20) which drives the atomic population down the ladder of vibrational states. It is possible to transfers essentially all the population to the ground state of the trap. However, in a lattice typically one does not observe a phase transition (e.g. to a Bose-Einstein condensate, see Sec. VI B) because there is less than one atom per potential well.

Another technique to cool atoms in a trap or optical lattice is to employ a dark state (see Box 6). Laser cooling in a standing wave laser field or optical lattice involving a dark state is referred to as grey molasses or a dark lattice and can produce slightly lower temperatures than optical molasses.

2) Evaporative cooling.

Neither sub-Doppler nor sub-recoil cooling are readily applicable to magnetically trapped atoms. Also the density limits imposed by near-resonant light requires that alternative cooling schemes be considered. If the density is sufficiently high that atoms undergo many elastic collisions before escaping, then they may be cooled by forced evaporation.

The process of evaporative cooling is similar to the cooling of a cup of hot and steaming liquid - the steam carries away heat leaving the liquid cooler. The principle at the atomic level is illustrated schematically in Fig. 21. In a collision between two atoms with roughly the same initial energies, the final energies have a range of possible values. If the hotter atom is allowed to escape, the net effect, after re-thermalisation, is to leave the remaining sample colder.

Collisions are the key component in evaporative cooling, without them evaporation would amount to no more than velocity selection, which does not increase the phase-space density. Runaway evaporation, where the collision rate is constant or increases, requires greater than 100 elastic collisions per trap lifetime

in a linear potential (greater than 400 in a parabolic potential, due to the weaker confinement). This threshold can be reached by transferring a laser cooled sample into a purely magnetic trap where extremely long lifetimes (a few minutes) are possible by reducing the background pressure and eliminating the possibility of spin-flip loss.

Another attractive feature of magnetic traps is the ability to eject atoms with a well defined energy by driving an rf transition to the untrapped state. This idea was first suggested as a technique to initiate evaporative cooling of magnetically trapped hydrogen and subsequently applied with great success to alkali atoms. The combination of magnetic trapping and evaporative cooling has allowed phase-space densities above quantum degeneracy to be achieved (see Sec. VI B).

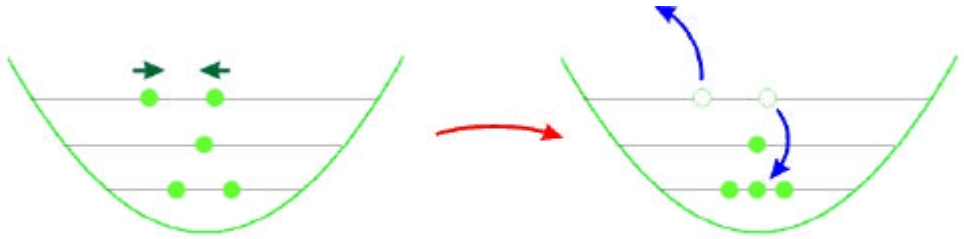

Fig. 21. *The principle of evaporative cooling. Two atoms, with the same initial energies, collide and scatter into different vibrational states. If the hotter atom is allowed to escape, the net effect, after re-thermalisation, is to leave the remaining sample colder. The temperature scales linearly with trap depth U ($k_BT \sim U/10$).*

VI. APPLICATIONS OF LASER COOLING AND TRAPPING OF NEUTRAL ATOMS

A. Precision measurement

The potential of slow atoms for precision measurements has been a significant motivating factor behind the developing laser cooling and trapping techniques. The prospect of improving the atomic clock or *frequency standard* is particularly appealing. The fact that the current frequency standard is based on the groundstate hyperfine transition in caesium, an ideal element for optical manipulation, is a fortunate coincidence.

The field of precision measurements is closely related to the development of fundamental SI standards. The standard for time (or frequency) is of particular importance and will set the strongest demands in the future. Consequently a great deal of work is going into improving the current standard and exploring the possibilities for a successor (Box 8 provides a brief history of clocks, and some notes on the implications for navigation, which still provides one of the main motivations for advances of this technology). Our ability to make electronic measurements of frequency is far superior to measurements relative to artefacts (e.g. the old standard meter or kilogram) or based on delicate set-ups (e.g. the ampere). The new definition of the meter is a good example, where by defining the speed of light, the artefact becomes redundant. For this reason, ongoing research is directed towards realising new standards linked to frequency measurements. For example, electrical standards are linked to frequency measurements via the Josephson frequency-to-voltage ratio $2e/h$. Finally, a range of fundamental experiments can be recast as frequency measurements and therefore, depend not only on the existence of a proper standard, but become, in themselves, frequency measurements with stringent demands on precision.

As a source for precision measurements, slow atoms have a number of advantages over room temperature vapours or thermal beams. The most obvious is the possibility of significantly longer interrogation times. However, the experimental implementation proved less than straightforward. In the original proposal for an improved caesium frequency standard (made in the early 1950's), Zacharias suggested aiming a thermal beam vertically (upwards) and set up an experiment sensitive only to atoms in the slow tail of the distribution

moving with velocities of 6 m/s or less. These atoms would turn around less then 2 m above the source and fall back down again under the influence of gravity. This would yield interrogation times of order 1 s, and the geometry also lends itself ideally to the application of Ramsey's technique of separated oscillatory fields (see Box 7 and Further Reading). In the Ramsey technique, the long interaction required to achieve high sensitivity is replaced by two short interaction regions separated by a long time. The fountain geometry provides the convenient simplification that only one interaction region is required because the atoms will pass through it on their way up and on their way down. Unfortunately Zacharias' experiments on atomic fountains did not work. It turned out that collisions with the faster atoms (the vast majority) effectively removed the slow tail.

Despite the failure of the experiment, the idea survived, and the collisions problem was finally solved in 1989 by the Stanford group who demonstrated the first atomic fountain based on laser cooled atoms. The idea was to trap and cool a sample of sodium atoms and subsequently launch them with a velocity of 2-3 m/s using light pressure. The experimental set-up is shown in Fig. 22. The groundstate hyperfine transition at 1.772 GHz was excited by the application of two short $\pi/2$ rf pulses (see Box 6) as the atoms were turning around inside a waveguide. Fig. 23 shows examples of the Ramsey fringe patterns (see Box 7) obtained in this experiment. The data shown in Fig. 23b represents 1000 s worth of experimental running time and allows the line centre to be determined to ± 10 mHz. For an interrogation time (i.e. time between the two rf pulses) of $\Delta T = 255$ ms the expected linewidth is $\Delta\nu = 1/2\Delta T \approx 2$ Hz as observed.

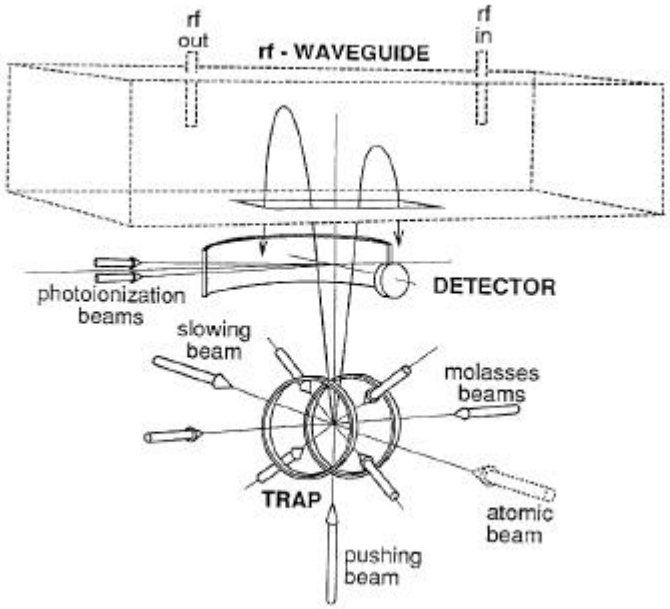

Fig. 22. *The experimental set-up used to produce a cold-atom fountain. The main components are the magneto-optical trap, the rf interaction region, and the detection region.*

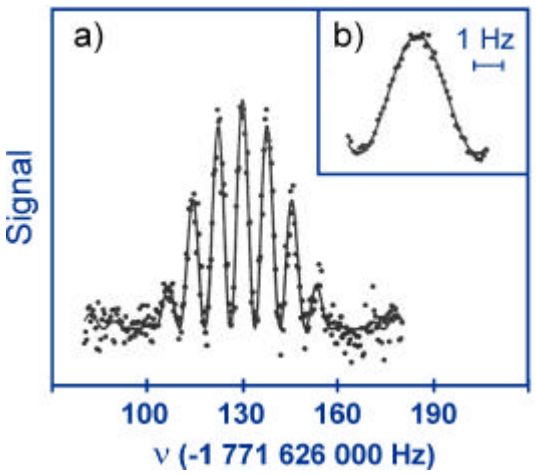

Fig. 23. *The observed rf signal in a cold-atom fountain. experiment. The fringes were produced by Ramsey's technique of separated oscillatory fields. (a) The transition is driven by two 32 ms rf pulses separated by 125 ms. (b) An expanded view of the central fringe obtained with two 3.2 ms rf pulses separated by 255 ms after 1000 s of integration.*

BOX 7

π−pulses and Ramsey fringes

As explained in Box 1 a two-level atom interacting with an external field (light or rf) performs Rabi oscillations, i.e. the population oscillates between the ground and excited state with the Rabi frequency ω_R. If the atom is initially in the ground state $|g\rangle$, and the external field is applied as a pulse lasting only half a cycle of the Rabi oscillation, the atom is transferred to the excited state $|e\rangle$. This is referred to as a π-pulse. Similarly, population initially in the excited state is transferred to the ground state.

If the interaction only lasts half as long as a π-pulse it is known as a π/2-pulse and the atom ends up in a coherent superposition of ground and excited states:

$$|\psi\rangle = \frac{1}{\sqrt{2}}\left(|g\rangle + e^{-i\omega_0 t}|e\rangle\right)$$

where $\hbar\omega_0$ is the energy difference between the states. The important point here is the phase difference between the ground and excited state components (represented by the factor $e^{-i\omega_0 t}$) evolves at a frequency given by the atomic transition frequency ω_0, i.e. the atom acts as a quantum mechanical clock.

This is the basis for a technique known as Ramsey's method of separated oscillatory fields used in atomic clocks. A time ΔT after the initial π/2-pulse is applied a second π/2-pulse is used to read out the atomic phase. If the oscillator driving the π/2-pulses has a frequency $\omega = \omega_0$ the second pulse is in phase with the atom and the combined effect of the two pulses is that of a π-pulse, i.e. the atom is transferred to the excited state. However, if the oscillator frequency is not exactly equal to ω_0, its phase slips relative to that of the atom and the excitation is in general no longer complete. If the frequency difference equals $\pi/\Delta T$ the second pulse is π out of phase and the atom is driven back to the ground state. At twice this frequency difference the second pulse again excites the atom, but the two oscillators have slipped by one period in the time interval ΔT. This gives rise to the characteristic Ramsey fringe pattern shown in Fig. 23.

This is similar to the interference fringes observed in a Young's double slit experiment where constructive interference is observed at points, where the difference in the number of oscillations for light travelling from the two slits equals an integer. Half way between these points of constructive interference the two fields are π out of phase and dark lines appear.

Subsequent work on Cs atomic fountains demonstrated the accuracy of the system, and begun to explore the limitations of the technique. The fountain has many advantages compared with traditional thermal beams. The obvious ones are the vast reduction in the observed linewidth and virtual elimination of the second-order Doppler shift, but just as important is the fact that many of the factors limiting the accuracy of thermal beam atomic clocks are significantly reduced. One example is the cavity phase shift error, which is the largest uncertainty in present Cs atomic beam clock. It is caused by the fact that the two Ramsey interactions take place in two separate cavities. Any phase difference between the two cavities will immediately translate into a shift of the observed line. In a fountain clock, there is only one cavity! The much reduced linewidth also means that the bias magnetic field required to isolate the correct clock transition ($m_F = 0$ to $m_F = 0$) can be reduced dramatically resulting in a reduced quadratic Zeeman shift.

Of the sources for systematic frequency shifts known from traditional atomic beam clocks, the bias magnetic field would appear to be the most severe in a fountain, limiting the accuracy ($\Delta\nu/\nu$) to the 10^{-16} level. This represents an improvement of 2-3 orders of magnitude compared to a thermal beam atomic clock (see Box 8). However, the use of cold atoms introduces new problems. The energy levels of colliding atoms shift, so if they shift differently for the two hyperfine levels of the clock transition, this will give rise to a density

dependent frequency shift. Shifts of several mHz have been observed for densities of order 10^9 cm^{-3}. However, the shift is linear in density and an extrapolation to zero density is feasible. With this correction an accuracy of 10^{-16} should be possible.

BOX 8 History of clocks

Year	Description	Stability
1656	Pendulum (Huygens)	10^{-3}
1760	Harrison[1)]	10^{-6}
1920	Master/slave pendulum (Shortt)	10^{-7}
1940	Quartz crystal (33 kHz)	10^{-9}
1960	Atomic clock[2)]	10^{-14}
1996	Atomic fountain clock[3)]	10^{-16}
2003?	*Cold atom clock (zero g)*	*10^{-17}*

1). *Harrison built five clocks: H1 (1735) accurate to a few seconds per day (~5 10^{-5}); H4 (1760) 5 s in 81 days (~7 10^{-7}); and H5 (1772) a pocket watch (accuracy ~4 10^{-6}). H4 was sufficiently accurate to solve the so-called longitude problem: 4 s is equivalent to ~1 mile at the Equator, therefore an accuracy of 10^{-6} corresponds to less than 1/4 mile after 1 month at sea.*

2). *The atomic clock was originally developed to test general relativity but it worked so well that in 1967 the second was redefined as 9,192,631,770 periods of the ground state hyperfine transition in ^{133}Cs. In addition, it has revolutionised satellite based navigation by facilitating the development of the Global Positioning System, accurate to 10 m. Ramsey, who developed the separated field technique, was awarded the Nobel Prize in 1989.*

3). *Chu, who worked on the first cold atom fountain, was awarded the Nobel Prize in 1997.*

It is interesting to consider the possibilities for improving the accuracy beyond the 10^{-16} level. There are essentially three routes: 1) improving the signal-to-noise ratio and our understanding of systematic shifts, 2) reducing the linewidth and 3) increasing the frequency. 1) is hard work! 2) represents an interesting option in a zero-g environment in particular because the most accurate clocks will be required for satellite navigation. 3) is a possibility for the future and will ultimately require a re-definition of the frequency standard. However, there are only a small number of atoms that can be laser cooled and have a possible clock transition.

As explained above, acceleration due to *gravity* is one of the limiting factors in an atomic clock. It is therefore interesting that the Stanford group has taken the ultimate revenge by turning an atomic clock into a device for measuring g with unprecedented accuracy. The principle can be understood as follows. The clock transition can be excited optically with a velocity sensitive Raman transition (see Sec. IV C). For given laser frequencies ω_1 and ω_2 the resonant velocity is:

$$\upsilon = \left(\omega_1 - \omega_2 - \Delta_{gs}\right) / 2k$$

If the beams are vertical the frequency difference required to maintain resonance with a given group of atoms will have to be varied linearly with time (proportional to g) as the atoms accelerate, according to $\upsilon(t) = g\,t$. It turns out there is no need to sweep the frequency difference. Instead, the light can be applied in three short pulses ($\pi/2$ - π - $\pi/2$, see also Box 7) with variable phase thereby creating an atom interferometer (see also Chapter by Pfau and Mlynek). From this point of view the technique measures the difference in gravitational potential between the two interferometer arms. An extremely high sensitivity to

gravity can be achieved. Fig. 24 shows a measurement of the variations of gravity recorded over a few days by a caesium interferometer at Stanford.

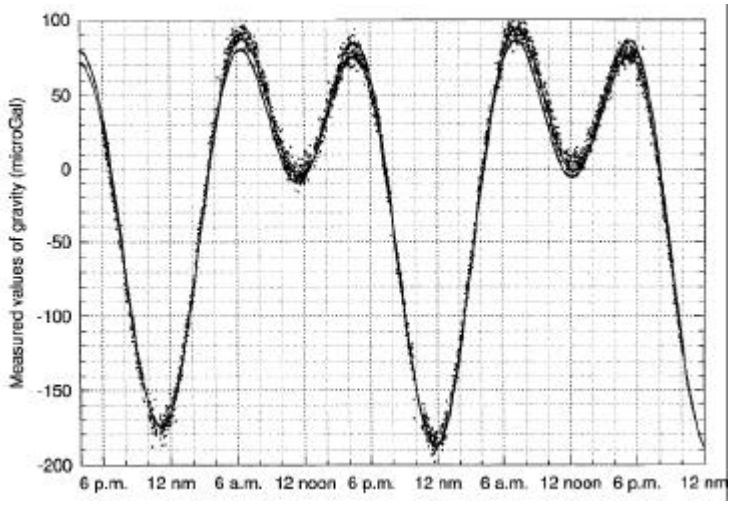

Fig. 24. *Continuous measurements of the gravitational acceleration g over a two day period using an atom interferometer. Each data point corresponds to a two minute measurement. The solid curves represent two different models of the Earth tides. (Figure courtesy of S. Chu).*

In the analysis of the dynamics of the photon absorption and emission processes in Section III B we were primarily interested in the conservation of momentum. The photon recoil, however, also has a measurable spectroscopic effect. An atom (or molecule) initially at rest will recoil with a velocity $\hbar\boldsymbol{k}/m$ so the equation for the conservation of energy will include a kinetic energy term corresponding to a shift of the absorption line. Similar conservation of energy arguments show that the resonance frequency for stimulating the atom back to the ground state again depends on the direction of the stimulating beam relative to the recoiling atom, such that two resonances occur separated by $2\hbar k^2/m$. An accurate measurement of this recoil splitting will therefore yield the ratio $\hbar/m$, which is of interest from a fundamental point of view, because in quantum mechanics mass only appears in this ratio.

The recoil splitting was first observed by Hall at JILA in saturated absorption spectroscopy of methane excited by a 3.39 μm HeNe laser. The exquisite velocity sensitivity provided by stimulated Raman transitions has allowed a precision measurement of this recoil splitting to be carried out by the Stanford group. The accuracy with which π-pulses can be applied has even allowed several additional absorptions and stimulated emissions to be included to increase the recoil splitting to 60 photons worth of momentum. Using a caesium atom interferometer similar to the one used in the *g*-measurement $\hbar/m$ has been measured with a precision of 10^{-7} in two hours of integration.

By using a combination of many of the techniques, that have been developed for laser cooling and trapping of neutral atoms, Hall recently measured the linewidth of the sodium cooling transition with high accuracy. The aim of this work was to resolve a discrepancy between calculated and measured lifetimes of the excited state. The traditional way of measuring lifetimes is to observe a fluorescent decay, which unfortunately suffers from a number of systematic effects related to the exact experimental geometry. Laser cooling allowed the lifetime to be determined from an accurate measurement of the natural linewidth of the transition. This measurement resolved the discrepancy and is in agreement with a recent and more careful measurement of the fluorescence decay.

One of the more exotic types of experiments made possible with laser cooled atoms is a test of parity violation. By combining measurements on several short-lived isotopes of caesium and francium, one can make an accurate comparison with theoretical calculations.

B. Quantum degeneracy

An important outcome of laser cooling and trapping is the dramatic increase in the phase-space density of the atomic sample. The phase-space density is the number of atoms per unit real space and momentum space, $n\lambda_{dB}^3$, where n is the number density and λ_{dB} is the thermal de Broglie wavelength. Physicists care about high phase-space density not only because, in general it increases the signal-to-noise ratio in most experiments, but more fundamentally because quantum mechanics predicts that remarkable things happen when the average particle separation, $1/n^{1/3}$, becomes comparable to the de Broglie wavelength, i.e., when $n^{1/3}\lambda_{dB} > 1$. In this regime, known as *quantum degeneracy*, the behaviour of bosons and fermions is dramatically different. For bosons the de Broglie waves of neighbouring particles interfere constructively such that all the particles condense in the lowest energy state forming a *Bose-Einstein condensate* (BEC). In contrast, the de Broglie waves of fermions interfere destructively such that the particles remain stacked up to a level necessary to accommodate just one particle per state.

Standard laser cooling and trapping techniques lead to a dramatic increase in the phase-space density, but not by enough to reach quantum degeneracy (see Fig. 25). The MOT is capable of producing temperatures as low as 10 T_{rec}, and densities up to 10^{11} cm^{-3} corresponding to a phase space density of order 10^{-5}. At this stage, the interaction with near resonant light becomes the limiting factor. Spontaneous emission causes diffusive heating and light scattering limits the maximum density. Marginally higher phase space density can be attained temporarily by compressing the MOT and cooling the compressed cloud using optical molasses (see Fig. 25). However, the pursuit of significantly higher phase space density requires the extinction of all near-resonant light. Consequently laser cooling and the magneto-optical trap must be abandoned. Instead, the atoms are transferred to a purely magnetic trap (discussed in Sec. V A), where the cooling is continued by forced evaporation (see Sec. IV D). A radio-frequency (rf) source selects atoms with a particular energy and transfers them to an untrapped magnetic sub-level. The temperature of the cloud is decreased by gradually lowering the selected energy by changing the frequency of the rf radiation. The decrease has to be slow to allow atoms time to re-thermalise. Both the temperature and the number of atoms are reduced by a few orders of magnitude, and if the initial atom number and density are sufficient, the phase space density can increase by the five orders of magnitude required to attain degeneracy.

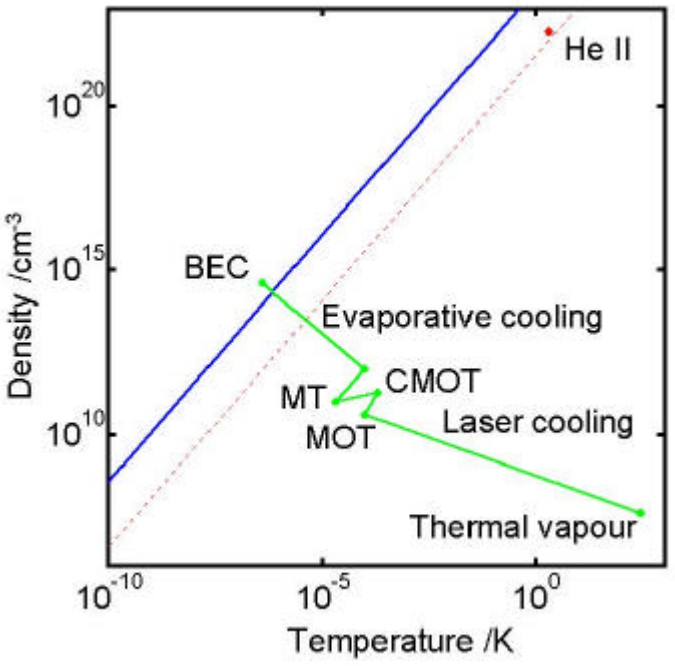

Fig. 25. *The route to BEC: Density against temperature plot illustrating how a Bose-Einstein condensate is produced using a sequence of laser cooling followed by evaporative cooling. The solid line, corresponding to* $\lambda_{dB} = 1.4\ n^{-1/3}$ *for* ^{87}Rb*, indicates the phase transition. The dotted line is the phase transition for* ^4He *The cooling sequence is as follows: 1. Room temperature atoms are laser cooled and confined in a MOT. The trap is compressed by increasing the magnetic field gradient (CMOT). 2. The magnetic field is turned off to allow a short period of sub-Doppler cooling (optical molasses) before transferring the cloud to a purely magnetic trap (MT). 3. The magnetic field is increased to compress the cloud. 4. An rf field is applied to evaporate hot atoms. The rf frequency is reduced until the transition to BEC (solid line) is crossed.*

The formation of a BEC using a sequence of laser and evaporative cooling was first observed in 1995 using rubidium by the group of Cornell and Wieman at JILA in Colorado; by Hulet and co-workers at Rice University in Texas using lithium; and by Ketterle and colleagues at MIT using sodium. In 1998 BEC was observed using hydrogen by Kleppner and co-workers at MIT using only cryogenic and evaporative cooling. The condensates consist of a few million atoms at a temperature between a few hundred nK and a few μK. The density can be greater than 10^{14} atoms per cubic centimetre, significantly higher than in laser cooling experiments. The formation of the condensate is marked by the appearance of a high density region at the centre of the atomic cloud. This high density region is easily detected by absorptive imaging using a near-resonant probe beam. Typical absorptive images are shown in Fig. 26.

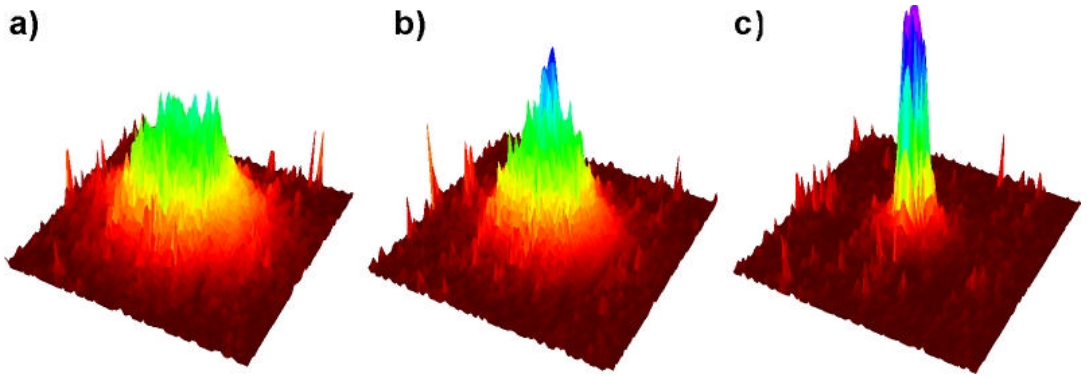

Fig. 26. *BEC at University of Sussex: Two dimensional probe absorption images showing the velocity distribution of sodium atoms released from a magnetic trap. The sequence shows the emergence of a Bose-Einstein condensate. The three images show a cloud cooled to: (a) just above the transition temperature; (b) just after the condensate appeared; and (c) well below the transition temperature where almost all the atoms are in the condensate. (Figure courtesy of A.S. Arnold).*

As BEC is a fundamental phenomenon underlying many key areas of physics, the first observation of the alkali vapour condensates was greeted with considerable excitement. The particular attraction of the dilute atomic condensates is that the density and temperature are sufficiently low that the theoretical description is relatively straightforward, allowing quantitative comparison between theory and experiment. Consequently, dilute BECs provide an ideal system for testing many-body theories. At low temperatures, atoms behave like hard spheres with a radius a (typically a few nanometers) known as the *scattering length*, and one can describe the collisions in terms of a mean-field, essentially an energy shift that depends on density. This mean-field description, leading to the *Gross-Pitaevskii* equation, has been shown to provide an accurate description of the shape and dynamics of dilute atomic condensates. The scattering length, a, may be either positive or negative corresponding to repulsive and attractive interactions, respectively. Attractive interactions tend to make the cloud collapse and condensates can be formed only for small numbers of atoms where the zero-point motion is sufficient to balance the attractive forces. Repulsive interactions cause the cloud to expand and change shape. The shape mirrors the trapping potential. In a parabolic potential the density distribution is parabolic, whereas in a square well potential, the density is uniform just like water in a bucket.

Some of the applications of atomic BEC include:

1. A Bose-condensate is an ideal source and may be thought of as the matter wave equivalent of a laser. The condensate is populated by 'stimulated scattering' into the ground state of the potential, similar to the stimulated emission of photons into a particular mode of a laser cavity. A pulsed output from a trapped condensate can be realised by driving a transition (rf or optical Raman) to an untrapped state. The coherence of the output has been demonstrated by interfering two initially separate regions of condensate. The strength of the analogy has led some physicists to adopt the term '*atom laser*'. However, it is not quite a laser in the sense that the pumping or loading and the output are performed sequentially. A continuous output would require continuous laser cooling and loading, which remains a

considerable challenge. However, one may envisage that even the first generation of '*atom lasers*' will make a significant impact in atomic physics, especially in the rapidly expanding area of atom optics, (see the Chapter by Pfau and Mlynek)

2. The dilute Bose gas is relatively simple *superfluid*. Experiments which probe the fluid dynmical properties, such as the formation and interactions of *quantised vortices* provide new insight into fluidity in general and quantum fluids in particular. To investigate the fluid properties, the laser manipulation techniques described in this Chapter prove very useful. For example, far-off resonant laser light may be used to split, excite, shape, pierce, and stir dilute alkali vapour condensates. Stirring leads to vortex formation. Vortices are an interesting entity which appear in wildly different areas of physics. Apart from their central role in fluid mechanics, and as fluxons in superconductors, they are related to cosmic strings, topological defects in space time thought to originate during the rapid expansion phase of the early universe.
3. The far-off resonant optical dipole traps discussed in Section V B may also be used to trap a condensate. The optical dipole potential also has the advantage that all the spin states are trapped simultaneously, and the magnetic field becomes a free parameter. This allows studies of *spinor condensates* and the possibility of changing the interactions by applying a uniform magnetic field. For example, if the magnetic field is varied such that a bound state in the interatomic potential moves into the continuum then the scattering length changes sign. This is known as a *Feshbach resonance*. By suddenly changing the sign from positive to negative, it is possible to investigate the dynamics of the condensate as it collapses.

Most of the alkali atoms used in laser cooling are bosons, but some isotopes such as ^{6}Li and ^{40}K are fermions. Laser and evaporative cooling of fermions leads to the formation of degenerate Fermi gases which have quite different properties to Bose condensates. One topic of interest is the possibility of fermionic pairing, where two fermions combine to produce a boson allowing a form of Bose condensation. This process is best known in the context of superconductivity where two electrons couple via a phonon to form a Cooper pair. For atoms, the pairing is predicted to occur at very low temperatures that are difficult to attain because the elastic collisions required for evaporative cooling are forbidden by the fermionic symmetry. One approach is to use a bosonic buffer gas to sympathetically cool the fermions. As in the case of dilute Bose condensates, dilute Fermi gases could provide new insight into diverse many-body problems, ranging from superconductivity to the stability of neutron stars.

VII. MANIPULATION OF MICRON SIZED PARTICLES

The versatility of laser manipulation is most clearly demonstrated by the broad range of particles that can be controlled, from atoms to small dielectric spheres (from tens of nanometers to tens of micrometers in diameter), viruses, living cells, and even organelles within living cells. The ability to attach small dielectric spheres as 'handles' on more complex molecules and polymers has extended the technique to a whole new class of particles. Furthermore, in addition to providing a means for moving particles around, lasers can also be used to *rotate* them. This is possible because in addition to the linear momentum considered so far, light can also posses *angular momentum*. Consequently, by optically tweezing a particle with a laser with angular momentum (circularly polarised) it is possible to set it in rotation.

In this Section we briefly discuss some applications from fields other than atomic physics, that have been revolutionised by the development of optical trapping techniques.

A. Basic ideas revisited and early work

The field of laser manipulation of micron sized particles was initiated by the pioneering work of Art Ashkin at Bell Laboratories on optical trapping of latex spheres (see Sec. III). A laser with power, P, impinging on a particle with reflectivity R exerts a radiation force $F = 2R\,P/c$, where c is the speed of light. For a laser

power of 1 W and a reflectivity of 10% this corresponds to a force of order 1 pN, which for a 1 micron diameter particle translates into an acceleration of a hundred thousand times that due to gravity. Initial work confirmed this estimate for the radiation pressure force but it was also observed that the particles suspended in a aqueous solution were attracted towards high intensity, providing the first experimental evidence of the optical dipole force. The dipole force, albeit more appropriately considered as refraction in an optical element (see Sec. III), would later become by far the more significant in the field of optical manipulation of micron sized particles.

In early experiments, dielectric particles were trapped against a wall (Fig. 27a) or in geometries where the scattering force was balanced either by a counter-propagating beam (Fig. 27b) or by gravity (Fig. 27c). In all cases trapping perpendicular to the beam axis results from the dipole force. A conceptually simpler and more robust trap is obtained by trapping all three dimensions using the dipole force (Fig. 27d). This single beam optical tweezer (see Fig. 3) relies on a strong backward dipole force downstream from a tight focus to balance the scattering force. The experimental geometry required for optical tweezers is easily realised with a conventional optical microscope by introducing the trapping laser beam in the optical path using a beamsplitter. This allows tight focusing, direct observation of the trapped particle, and control of the trap position within the viewing area by external optical adjustments.

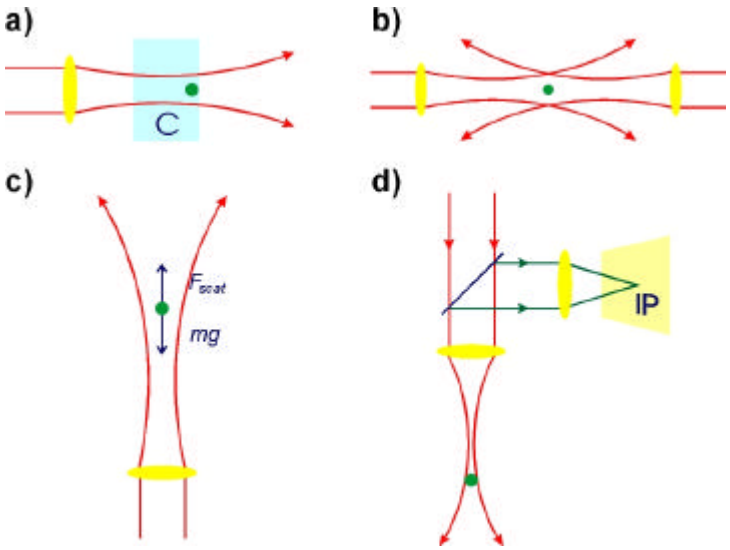

Fig. 27. *Trapping of micron sized particles. a) A particle in a cell (C) is attracted to the centre of the weakly focused laser beam by the dipole force and pushed along to the end of the cell by the scattering force. b) The scattering forces from two counter propagating beams cancel and the particle is held in a two-beam optical trap. c) The scattering force is counterbalanced by gravity in the levitation trap. d) The particle is trapped in three dimensions by the dipole force from a tightly focused laser beam. This configuration known as optical tweezers is typically obtained by sending the trapping light through an optical microscope. The fluorescence from the sample can be viewed in the image plane (IP).*

B. Applications of particle trapping in Biology

1) Manipulation of cells and organelles within cells

The application of optical tweezers to the manipulation of biological samples began with Ashkin's study of the trapping of tobacco mosaic viruses using a blue-green argon ion laser. The rod-like viruses were in an aqueous solution and were observed to align in the focused laser beam and stay trapped for tens of minutes without any apparent optical damage.

During the course of these experiments an unintended but highly important discovery was made. After the virus samples had been left for a few days strange new particles appeared moving around in the solution. They were identified as tubular micron sized bacteria propelled by rotating tails and were readily trapped in the optical tweezers at relatively low powers. However, optical damage was apparent at even modest powers - the bacteria were 'opticuted'. This problem was readily solved by changing the trapping laser to a Nd:YAG laser operating in the infra-red, where the absorption of living cells is significantly lower.

With this set-up a series of spectacular experiments were reported showing the revolutionising potential for this technology for manipulation of live cells. It was possible to hold yeast cells and E. coli bacteria in tight traps for hours. It was even possible to observe the cells multiply in captivity and to manipulate internal organelles within trapped protozoa. This demonstrated the inherently non-invasive nature of the technique. By introducing a second trapping beam it was possible to manipulate and orient elongated cells.

Experiments soon moved on from demonstrations of a novel effect to examples of novel measurements and potential treatments based on laser manipulation of biological samples. Examples include measurements of the torsional compliance of a bacterial flagellum and the use of optical tweezers in *in vitro* fertilisation to insert sperm directly into an egg.

2) Manipulation of single molecules

Many of the recent biological applications of optical tweezers have concentrated on manipulation of single molecules. One key area pursued in particular by Steven Block, now at Princeton, is the study of molecular motors. At the single cell level, movement (muscle action, cell movement or transport of organelles within cells) takes place as a mechanoenzyme turns chemical energy into movement. By attaching micron sized dielectric spheres to the molecules and then manipulating the spheres it has been possible to track the movement of a single mechanoenzyme along a microtubule. This has also allowed measurements of the tiny force of this most basic molecular motor (a few piconewton!), and observations of how the motor takes small steps (about 10 nm) and detaches itself during part of each cycle. This work, in turn, has stimulated new models of the kinetics of the enzymes.

The transcription of a DNA molecule, one of the most basic processes of life, has also been studied using optical trapping. During transcription a single RNA polymerase enzyme moves along a strand of DNA assembling free ribonucleotides into messenger RNA. By attaching the RNA polymerase to a microscope cover slip and optically tweezing a polystyrene bead attached to the end of a DNA strand it was possible to observe the RNA polymerase drag itself along the DNA, stretch it out and eventually stall. Despite their similar behaviour, RNA polymerase bears very little resemblance to mechanoenzyme. One significant and surprising difference is that RNA polymerase is much stronger! The force exerted by the molecule was measured to be 14 piconewton.

C. Applications to polymer physics

In an interesting extension of the work on biological samples, the DNA molecule has been studied as an example of a basic physical system, the polymer. A concentrated solution of polymers has rather interesting mechanical properties. On a long time scale it behaves like a viscous liquid, while on a medium time scale it is more like rubber, and on a short time scale more like a solid. This behaviour was explained about 20 years ago by the 'reptation' model of de Gennes. His basic assumption was that a polymer within a dense solution is confined by the remaining entangled polymers to move along a tube defined by its own contour. Consequently each individual polymer moves by one-dimensional diffusion along this tube such that the ends slide through solution like a snake - hence the word 'reptation'. This restricted movement is responsible for the material's inability to deform on the short time scale, while the slow diffusion along the tubes results in the long-term viscous properties. The characteristic time scales separating these regimes is determined by the length of the individual polymer chains.

From a physical point of view DNA is an ideal polymer. It has the added advantage that it is one of the most studied systems and techniques exist for selecting individual strands varying in length from very short up to hundreds of thousands of base pairs. In a series of experiments with individual fluorescently stained λ-phage DNA in a dense solution of unstained molecules Steven Chu and collaborators at Stanford University demonstrated this basic tube-like motion of the polymer (see Fig. 28). They were also able to measure the time scales involved in the relaxation of polymers of various length after having been deformed. A universal scaling with the polymer length L of the slowest relaxation time τ was found to be $\tau \propto L^{1.66\pm0.10}$, in

qualitative agreement with the reptation model. The key to performing these experiments was the ability to manipulate one end of the stained DNA molecule by attaching a micron sized polystyrene bead.

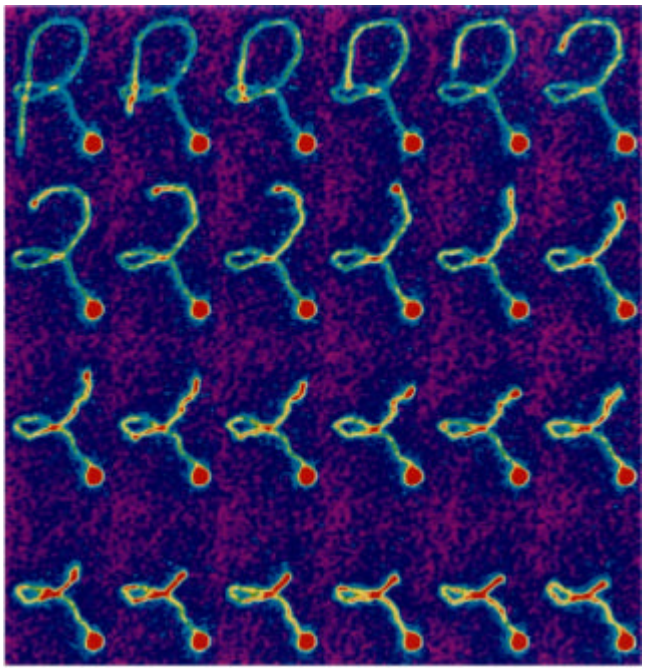

Fig. 28. *The relaxation of a strand of fluorescently stained DNA in a concentrated solution of unstained molecules. One end of the DNA is attached to a micron sized polystyrene sphere, which is held by optical tweezers (bright red spot). The series of images shows how the DNA relaxes along its own path demonstrating the tube-like motion enforced by the entangled polymers in the solution. (Figure courtesy of S. Chu).*

VII. CONCLUSION

In this Chapter, we have seen how the development of lasers has greatly enhanced our ability to control the motion of neutral particles. In atomic physics laser are used to cool atoms to within a millionth of a degree above absolute zero – the coldest temperatures produced by any technique. This has led to a range of novel developments, most notably in precision measurement such as a new generation of atomic clocks and the emergence of an entirely new area of research, the Bose-Einstein condensate. However, the impact of laser cooling has been felt well beyond the atomic physics research laboratory. Lasers can be used to trap and manipulates particles from atoms up to micron sized dielectric spheres and living cells. Research with optical tweezers has shed new light on fundamental biological processes at the molecular level and promises advances in medical treatment.

In a mere couple of decades, laser cooling and trapping has matured from a fundamental research topic of a few groups internationally to an established technology, with a major impact in areas of physics, chemistry and biology. This revolution will no doubt continue and grab the scientific headlines in years to come, as the range of applications widen and more astonishing discoveries emerge from the fundamental interaction between light and matter.

VIII. FURTHER READING

General:

S. Chu, Science, **253**, p. 861, 1991; and C. J. Foot, Contemp. Phys., **32**, p. 369, 1991. *Additional material at a introductory level.*

S. Chu, C. Cohen-Tannoudji, and W. Phillips, Rev. Mod. Phys. **70,** p. 685-741, 1998. *The three Nobel Laureates describe the historical development of laser cooling and trapping.*

C. S. Adams and E. Riis, Prog. Quant. Electron. **21**, p. 1, 1997. *More technical detail and references to original papers.*

A. Ashkin, Proc. Natl. Acad. Sci. USA, **94**, p 4853, 1997. *Comprehensive review by one of the pioneers of the field with emphasis on both physical and biological applications.*

The light radiometer:

F. S. Crawford, Am. J. Phys. **53**, p. 1105 (1985). *Describes how it is possible to run Crookes' Radiometer Backwards.*

Lévy flights:

C. Tsallis, Phys. World **10** no. 7 p. 42 (1997).

Earnshaw's theorem:

W. Earnshaw, 'On the nature of the molecular forces which regulate the constitution of the luminferous ether.', Trans. Camb. Phil. Soc., **7**, p. 97 (1842).

Atomic clocks and Ramsey fringes:

W. M. Itano and N. F. Ramsey, Sci Am. p. 46 July 1993.

N. F. Ramsey, Rev. Mod. Phys., **62**, 541 (1990).

Bose-Einstein condensation:

Science **269,** 14 July, 1995. *Reports the breakthrough on BEC.*

K. Burnett, Contemp. Phys., **37**, p. 1, 1996. *Describes the physics underlying BEC in more detail.*